ATLAS

October 12, 2009

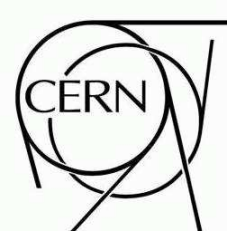

Results from 2008 Cosmic data analysis of ATLAS Muon Spectrometer

Draft 1

*) See following pages for the list of authors

Abstract

In fall 2008 the ATLAS detector has been operated for several months. In addition to a few days where the LHC beam has been circulated in the machine extensive running periods with cosmic ray acquisition have been performed. In this paper a collection of results from the ATLAS Muon Spectrometer derived from cosmic ray runs are reported. The main goal of the studies reported in this paper has been the understanding of the performance and the commissioning of the Muon Spectrometer. Several aspects that contribute to muon reconstruction performance have been studied in details going from detector coverage, single hit efficiency and resolution, calibration, alignment, segment and track reconstruction efficiencies.

(To be submitted to Nuclear Instruments and Methods)

1 Introduction: The ATLAS muon spectrometer

Editor: F. Cerutti

The ATLAS muon spectrometer (MS) has been designed to provide standalone measurement of the muon momentum with a relative ranging from about 3% to about 10% at 1 TeV and to trigger on single muons with transverse momentum down to a few GeV. A more detailed description of the ATLAS muon spectrometer and of its expected performance can be found in [1] [2] [3]. Here only a brief overview is given. The muon momentum is determined by measuring its curvature in a toroidal magnetic field. The magnetic field is provided by three toroids (one in the barrel and one for each end-cap), with a typical field integral in the range between 2 and 8 Tm. The muon curvature is measured by means of three precision chambers positioned along its trajectory. In order to meet the required precision in the very high momentum region each muon station is expected to provide a measurement of the muon trajectory, in the precision plane, with an accuracy of the order of 50μm. For most of the acceptance the precision chambers consist of Monitored Drift Tubes (MDT). In this paper the coordinate perpendicular to the wire, measured by the MDT, is referred to precision or bending coordinate being mainly perpendicular to the direction of the toroidal field. In the end-cap inner region, for pseudorapidities greater than 2, the Cathode Strip Chambers (CSC) are used since they are able to cope with higher background rates, at the expense of an increased electronics channel density.

The trigger chambers are based on two different technologies: the Resistive Plate Chambers (RPC) are covering the barrel region while the Thin Gap Chambers (TGC) are used in the higher background environment of the end-cap region. Two RPC chambers are attached to the middle barrel chambers providing the low-P_T trigger information. The high-P_T trigger is provided by the RPC modules installed on the outer barrel chambers combined with the middle chambers signals. The RPC are also used to provide the coordinate along the MDT tubes that cannot be measured by the MDT chambers.

Similarly in the end-cap two TGC doublets and one triplet are installed close to the middle station and provides the low- and high-P_T trigger signals. The TGC are also measuring the coordinate of the muons in the direction parallel to the MDT wires. In this paper this coordinate is referred to as second or non-bending coordinate. To this purpose some TGC chambers are also installed close to the inner MDT to improve the measurement accuracy of this coordinate.

Some MS naming conventions adopted in this paper are introduced here. The MS is divided in the XY-plane (also referred to as phi-plane) in 16 sectors being sector 5 the upper and sector 13 the lowest ones. In both Barrel and End-cap regions the precision chambers sectors are divided into 6 Large sectors (odd sectors) and 6 Small sectors (even sectors). In relation with the distance from the nominal Interaction Point the Muon Precision Stations are named Inner, Middle and Outer. Along the beam (z) axis with respect to the Interaction Point the MS is divided into 2 sides called side A and C.

As a complementary source of information to this paper the two publications [4] [5] on the MS system test performed previously to the MS installation in the CERN north test beam area can be consulted.

In the 2008 fall period the ATLAS detector has been operated for several months. The first beam where circulated in the LHC machine but no beam-beam collisions where delivered. The ATLAS detector has been collecting during this period mainly cosmic runs. The cosmic trigger of the data analyzed in this paper was based on the muon trigger chambers and is briefly described in Section 3. The analyzed data samples and the reconstruction software used in this paper are described in Section 2. Studies of Muon Spectrometer (MS) data quality, calibration, alignment and performance are presented in Sections 4, 6, 5, 7, 8 and 9 respectively. The conclusions are derived in Section 10.

2 Data Samples and Reconstruction Software

Editors: Rosy, Kevin and Niels

2.1 Samples

In preparation for collisions from the LHC, the ATLAS detector has acquired several hundred million cosmic ray events during several run periods in 2008 and 2009. In this paper a subset of data corresponding ot abut 40 M events has been analyzed. These runs allowed for the ATLAS detector, trigger, data acquisition, and reconstruction software to be commissioned. Most of the cosmic rays reach the ATLAS experiment via the two big shafts. They have incident angles very close to the vertical axis and they are mainly triggered by the Barrel trigger chambers (RPC). The selected runs together with the status of the B field in the muon spectrometer and the number of collected events for the different trigger streams are listed in Table 1.

Run Number	Trigger Stream	B Field	Number of Events
91060	RPC	Off	17M
91060	TGC	Off	0.2M
89106	TGC	Off	0.4M
89403	TGC	Off	0.4M
91890	RPC	On	16M
113860	RPC	Off	6M

Table 1: List of analyzed data runs together with the correspondent trigger stream statistics and status of the muon spectrometer toroidal magnetic field. All runs were collected in fall 2008 with the exception of run 113860 collected in spring 2009.

2.2 Muon Reconstruction Software Overview

The runs collected during this period were analyzed using the ATLAS software chain in several steps. The data were processed following several steps: data decoding, data preparation (that includes calibration and alignment) and track reconstruction. The first two items are discussed in some detail in Sections 5 and 7. Muon reconstruction has been handled by two independent packages namely *Moore* and *Muonboy* [1], [7], which are fully integrated into the general ATLAS computing environment [6]. The two reconstruction algorithms are similar in design but differ in some detail. The general strategy is to reconstruct track trajectories both at a local (individual chamber) as well as at global (spectrometer wide) level. The trajectories which are reconstructed at the individual chamber level can be approximated as straight lines over the short distance they traverse and are therefore fit to straight line segments (referred to as *segments*. Full tracks are formed by combining segments from multiple chambers.

Prompt muons produced from proton-proton collisions will have trajectories that point back to the Interaction Point (IP) where the collision occurred. The detector front end electronics will receive the timing signals (25 ns clock) for the LHC machine and they will be synchronous with the collision time. In contrast, cosmic ray muons are 'non-pointing' and are not synchronous with the detector clock (i.e., they have an additional 25 ns jitter with respect to the clock selected by the trigger system). In addition during the commissioning the different trigger systems were not fully timed in leading to variations in the timing depending on the region of the detector that has originated the trigger. A further complication was due to the not final alignment of the muon spectrometer as discussed in Section 7. The reconstruction algorithms were adapted for these conditions as described below. For both programs this involves enlarging the uncertainties on the individual hits, relaxing standard tracking requirements, and implementing a procedure to accommodate the cosmic-ray timing conditions. As stated above, the cosmic

rays being not synchrounous with the LHC clock will introduce an additional time jitter of 25 ns that will degrade the space resolution of the MDT chambers. A procedure called $t_0$refit has been developed by both reconstruction algorithms. The general philosophy beyond this procedure is to determine with higher accuracy the time in which the cosmic ray inpinged on the detector by leaving the t_0 parameter free in segment reconstruction. The actual implementation of the t_0-refit in the two main reconstruction codes is briefly described below while the achieved performance are detailed in Section 5.

2.3 Muonboy

The strategy of the *Muonboy* reconstruction algorithm can be summarized in four main steps:

- Identification of Regions Of Activity (ROA) in the muon system, through the RPC/TGC systems;
- Reconstruction of local segments in each muon station in these regions of activity;
- Combination of segments of different muon stations to form muon track candidates using three-dimensional tracking in the magnetic field;
- Global track fit of the muon track candidates through the full system using individual hit information.

The topology of cosmics is addressed by relaxing the ROA requirement (segments and tracks are looked for in the whole region of the MS) and the pointing criteria when looping on hit pairs while making segments or when matching segments while fitting tracks. Since the detector is not fully commissioned and validated and most events are very low occupancy much looser requirements are made in the selection of both segments and tracks. To cope with the not fully commissioned trigger timing and with the natural time jitter of cosmics with respect of the LHC clock the t_0 parameter of each station has been added as a free parameter in the segment fit procedure (the so called t_0-refit procedure explained in Section 5). In the Muonboy algortihm the t_0-refit procedure consists into a scan of different t_0 values in steps of 10ns, doing a full segment reconstruction on each one. The t_0 value giving the best reconstruction quality factor is kept, and a parabolic fit is performed using this best value, the preceding one and the following one. The t_0 corresponding to minimum of the quality factor parabola is kept. In order to keep high efficiency for track reconstruction in cosmic events the MDT single hit resolution is enlarged by adding in quadrature to the expected intrinsic resolution (described in Section 6.1) a 500 μm smearing. This smearing is increased by additional 500 μm if the t_0-refit procedure described above fails. Another criteria that is relaxed in cosmic ray events reconstruction is the penalty factor related to missing associated hits on the track trajectory (hits that are expected but are not found).

2.4 Moore

The *Moore* reconstruction algorithm is built out of several distinct stages:

- Identification of global roads throughout the entire spectrometer using all muon detectors
- Reconstruction of local segments in each muon station seeded by the global road
- Combination of segments of different muon stations to form muon track candidates
- Global three-dimensional tracking and final track fit

Several modifications to the standard pattern recognition were made to optimally reconstruct cosmics. In the global-road finding step a straight line *hough transform* is used to allow for non pointing tracks. Cuts on distance and direction between the road and segment were relaxed. In the segment finding no

cuts were applied on the number of missing hits (tube that are expected to be crossed by the segment but without measured hits). The t_0-refit consists in varying simultaneously the time offsets (t_0) of all hits involved in the segment reconstruction. Each t_0 value is translated into a set of drift radius via the $r(t)$ relation. The t_0 value that minimizes the sum in quadrature of the weighted residuals (corresponding to the segment reconstruction χ^2) is selected. This fit is performed only for segments with MDT hits on both sides of the wire. In this fit the MDT drift errors are set to two times the nominal tube resolution. If the segment fit is not successful a straight line fit is performed assuming a 1 mm error without any drift radius dependency. Hits are removed for the segment if they are more than 7σ away from the track. In the track fit the MDT drift errors are enlarged to 2mm to take into account uncertainties in the station alignment alignment. Finally, a cosmic track is only split into two tracks at the perigee (point of closest approach to nominal ATLAS Interaction Point in the xy plane) if the track crosses the barrel calorimeter volume.

3 Trigger configuration during cosmics data taking

A more detailed configuration of the ATLAS trigger system can be found in [3]. Here only specific issues related to the 2008 cosmic data taking are briefly described. The muon level-1 trigger is issued by the RPC detector in the barrel ad by the TGC detector in the end-caps. During the 2008 cosmic-ray data taking, the MS has been the main source of the Cosmic ray trigger. A special MS trigger configuration has been adopted to allow the commissioning of the muon trigger system (both in terms of detector coverage and timing as explained later in the paper) while collecting cosmic ray statistics needed by the other sub-systems of the ATLAS detector. In *beams collision* configuration, level-1 muon trigger estimates transverse momentum in six deifferent p_T thresholds and send information to the Central-Trigger-Processor (CTP). The six threshold, three low-p_T and three high-p_T, do not distinguish between the different detector regions (Barrel and End-caps). In the cosmic runs analyzed in this paper it was chosen to keep 3 thresholds for the Barrel and 3 for the End-cap separately to help the commissioning of both systems. For the cosmic runs considered in this paper the higher level triggers (level-2 and Event Filter) where not used to reject events.

3.1 Barrel Level-1 configuration

In the runs analyzed in this paper only a coarse time alignment was in place. In the bottom sector, the last to be commissioned, in addition to a very coarse global time-alignment (difference in time for cosmic triggers generated by different sectors) also the sector internal time-alignment was very preliminary (difference in time for triggers generated by different trigger towers of the same sector). Moreover only on few sectors both the eta (bending coordinate) and the phi (non-bending coordinate) views were timed in. For this region only the phi view has been used in the barrel trigger. The trigger required a majority logic of 3/4, i.e. the trigger logic requires a time coincidence of at least three phi hits out of the four low-p_T trigger layers. For the high-p_T the requirement was to find hits in at least one of the two outer stations layers in coincidence with the result of the low-p_T one. To emulate as much as possible the timing expected from beam collisions and optimize the acceptance of the ATLAS Inner Detector, the cosmic-ray trigger was issued by mainly by the bottom sectors since the top sectors were delayed by 5 BC (125 ns) to reduce their chances to produce a level-1 trigger.

The trigger configuration from the geometrical point of view (*trigger roads*) was such that no requirements on the eta plane was present. A trigger roads were applied on the phi view. As explained above of the six available thresholds three were assigned to the Barrel and three to the End-cap. The 3 threshold used for the barrel were MU0_LOW, MU0_HIGH and MU6. The two threshold MU0_LOW/HIGH do not correspond to a physical p_T range; in fact, they are triggered by the time coincidence of hit on 3 out

of 4 planes without any geometrical requirement. They are also referred to as *open road*. The threshold MU6 on the contrary was using the real geometrical constraint for pointing muon of 6 GeV, but due to the fact the we were using only the constraint in phi and not in eta, the bending plane, it was actually not selecting the p_T of the muons. In the runs analyzed in this paper the high-p_T trigger was not yet commissioned, the time alignment of the low-p_T trigger was not yet completed and the data-readout latencies were not optimal. The largest impact on the RPC detector coverage comes from the readout latencies: the hits on the high-p_T planes that were not timed in were lost in the readout and therefore this implied a loss of efficiency. The situation has largely improved in runs taken in spring 2009 both in terms of detector coverage and in timing and trigger set-up , as shown in Sections 4.2 and 6.2.

3.2 End-cap Level-1 configuration

During fall 2008 running period the TGC trigger system has provided three types of triggers, named *MU0_TGC_HALO*, *MU0_TGC* and *MU6_TGC*. The trigger scheme is based on the coincidence logic between several layers of TGC gas-gaps. The main differences between these three trigger items are related to the required number of layers and to the level of pointingness to the ATLAS Interaction Point (IP). The first item *MU0_TGC_HALO* requires 3 out of 4 layers coincidence in the 4-layers that are more far away from the IP in both eta (bending) and phi (non-bending) view with a pointing requirement of $\pm$20 degrees. The other two items, both *MU0_TGC* and *MU6_TGC* require 2 out of 3 layers coincidence in the 3-layers TGC layers closer to the IP in eta view. The pointing requirement of *MU0_TGC* is of less than $\pm$10 degrees while for *MU6_TGC* is of $\pm$5 degrees. The trigger timing was aligned as for the high-momentum muons coming from the IP. All the delays due to different Time-Of-Flight and cable lengths (more than 10k cables) were properly set and cross-check using a test pulse system achieving a timing at a level of 4ns. For most of the 2008 cosmic run period, only the level-1 triggers generated from bottom part of TGC was used in the data taking. This was chosen to avoid the cosmic muons (coming mainly from the ATLAS shafts) that crosses first the top of one TGC wheel and later the bottom of the opposite ones would be triggered by the former being out of time in the inner detector with respect to muons coming from collisions.

4 Detector Coverage and Data Quality assessment

4.1 The Precision Chambers: MDT

The data quality framework of the ATLAS MDT system consists of several parts working on different stages of the data taking procedure. The Detector Control System (DCS) is the first source of information available during the operation of the detector. Here information about the hardware status of the different sub-detectors as well as all settings of the Low Voltage (LV) and of the High Voltage (HV) power and gas supply is available. The DCS also receives notes from the data acquisition (DAQ) as soon as problems during the readout of a chamber appear.

The next participant in the chain of data quality assessment is the on-line monitoring. It receives its input from the data acquisition system running in a spectator mode. Once the data are decoded monitoring histograms are filled showing quantities related to the detector operation.

In order to increase the available muon statistics part of the muon data, via a special stream that select muon chambers hit in the level-1 region of interest before the level-2 trigger decision, are transfered to three dedicated computing centers (referred to as *calibration centers*), which have been set up to determine and monitor the calibration parameters of the MDT chambers. In the calibration centers large statistics is available, which allows a more detailed look at quantities per electronic readout channel. The goal of the analysis performed at the centers is to provide feedback to the detector operation within 24 hours.

On a longer time scale, using the full reconstructed ATLAS event information, the off-line data quality monitoring provides the final information about the data. At each of the mentioned steps a flag summarizing the knowledge about the data quality at this level is produced and stored in a database.

In the run 91060 all MDT chambers had been installed (with the exception of the EE chambers that have been staged and are expected to be installed in 2009-2010) and used in the readout. Due to the cosmic ray illumination, geometrical effects and trigger coverage not all chambers had sufficient statistics to determine performance at single tube level. The studies reproted here have been performed on different levels of detail starting with per chamber information down to per tube information. Out of 1110 MDT chambers only five MDT chambers were not included in the data taking for run 91060. Of these 5 chambers two were not yet fully connected to services. The other three chamber were excluded due to problems with the gas system.

The studies performed on the data search for problems of individual readout channels as well as of clusters corresponding to hardware related group of tubes. A screen shot of one of the monitoring application used for the MDT system is shown in Figure 1. The the median number of hits per tube for each MDT chamber is plotted. The five chambers not included in the data taking are marked by dark gray boxes. Two more chambers are visible with very low statistics due to problems with the correspondent HV channels . For other 32 MDT chambers one of the 2 multi-layers had no HV.

The full MDT system consists of $\sim$ 340k readout channels of which $\sim$ 1.5k belong to the chambers not included in the readout. Out of the remaining channels $\sim$ 1k correspond to malfunctioning hardware or gas problems. These problems can easily be spotted already by the on-line monitoring. Problems in the gas system or the HV power supply affect one or more tube-layers of one MDT chamber. In 20 cases problems in the readout hardware affecting eight to 24 tubes have been found. Beside these clusters of tubes with problems, 323 individual dead readout channels have been found. The cosmic ray integrated flux was not sufficient for a detailed analysis at the single tube level for 15 MDT chambers (about 3k channels) so only 336k channels out of 339k were analyzed at the single- tube level.

Number of analyzed channels (enough expected statistics)	336144	100%
Channels not included in the readout	936	0.28%
Other channels with readout or initialization problems	744	0.22%
Channels with HV or gas problems	2942	0.88%
Permanently dead channels (broken wires)	323	0.10%
Total Problematic channels	4945	1.47%

Table 2: List of MDT channels with problems in run 91060.

A detailed list of problematic channels for run 91060 is reported in Table 2 together with the corresponding fraction relative to the total number of expected channels. To summarize about 5k channels out of 336k had shown some problems in run 91060, corresponding to 1.5%. Most of these channels has been recovered during 2008-2009 shutdown period. Only a very small fraction of problems, at the few per mill level, could not be solved like permanently disconnected tubes (broken wires) and chambers with very difficult access.

4.1.1 Results from MDT Offline Monitoring

In addition to monitoring performed in the DAQ framework (online monitoring) the collected ATLAS data are also processed with the offline reconstruction program and monitoring histograms are produced. This step is fundamental to ensure that the reconstruction works properly and correct conditions data (calibration and alignment) are used in the first processing of the data. As an example MDT hit-level

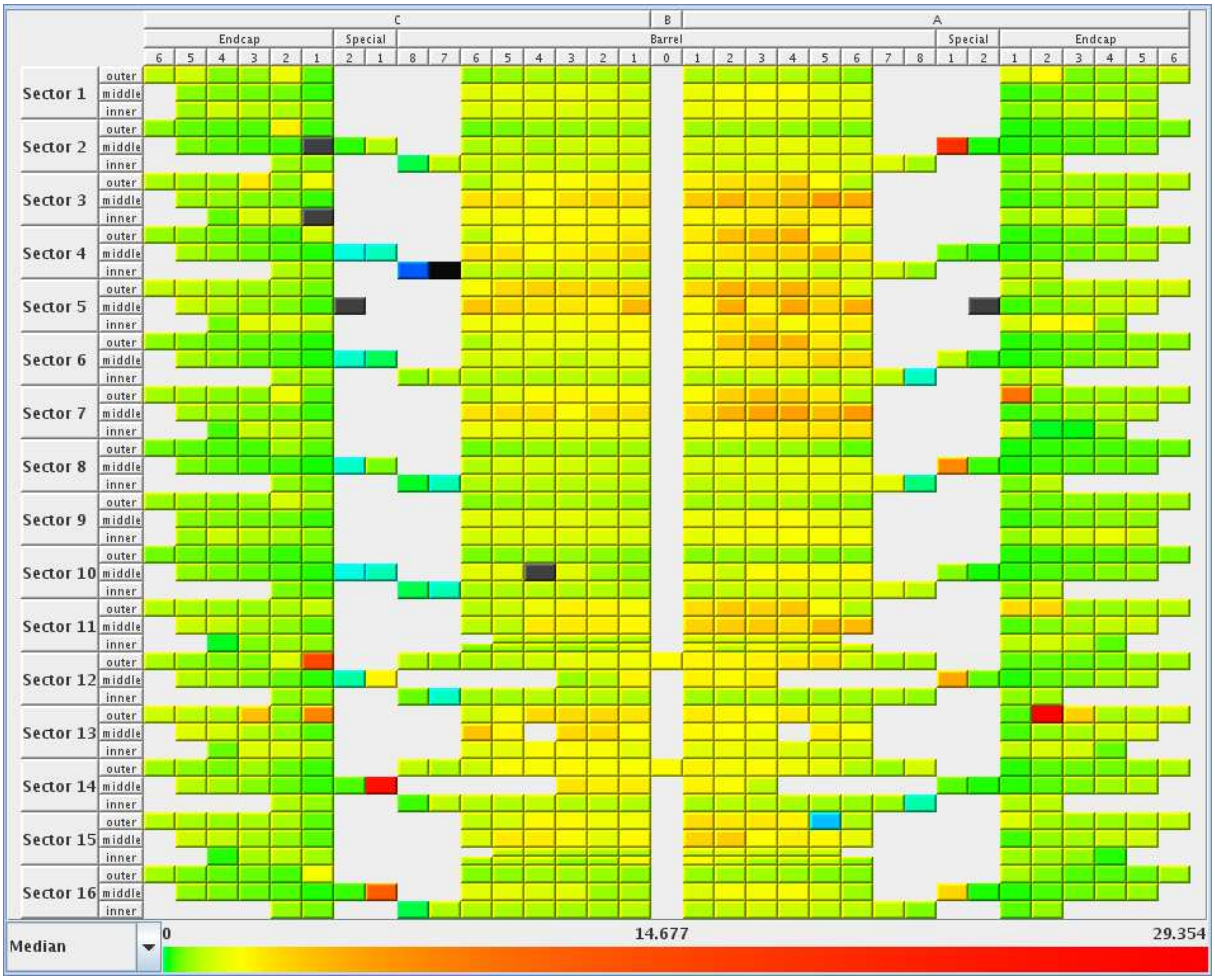

Figure 1: Screen-shot of a monitoring application displaying the MDT hit occupancy for all ATLAS MDT chambers. Each chamber is represented by a small box. The color of the box is related to the median number of raw hits per tube in that MDT chamber in logaritmic scale. The boxes are arranged in a grid, in which a column represents a slice perpendicular to the ATLAS beam axis. The rows are grouped into the sixteen sectors of the ATLAS MDT system. Within each sector chambers of the Outer, Middle and Inner ring of chambers are displayed.

monitoring from offline gathers and presents information on MDT hit-level variables, which include TDC and ADC spectra, drift-time measurements, hit occupancies per chamber multi-layer, and noise rates. These variables are obtained for individual MDTs and for various regions of the detector geometry, such as eta station, phi sector, barrel, end-cap, side A or C. In addition to pure hit-level variables reconstructed quantities related to segments and tracks are monitored. An example of histograms produced by the MDT offline algorithms are shown in Figure 2. In this plot the number of hit per multi-layer for run 91060 are shown. In the vertical scale the 16 phi sectors for multi-layers 1 (from 1.00 to 1.15) and 2 (from 2.00 to 2.15) are plotted while on the horizontal axis the 12 eta towers (from -6 to -1 for side C and from 1 to 6 for side A) of the Barrel Middle stations are shown. The missing multi-layers for eta values between 3 and 6 (both negative and positive) and for phi values are on 1.11, 1.13, 2.11 and 2.13 corresponds to the unistrumented region in the feet of the ATLAS toroid. The only multi-layers not active in the barrel Middle chambers correspond to the two holes at phi 1.09 ans 2.09 and eta -4. This

MDT chambers, BMS4C10, had readout problems during this run and therefore no hit were recorded.

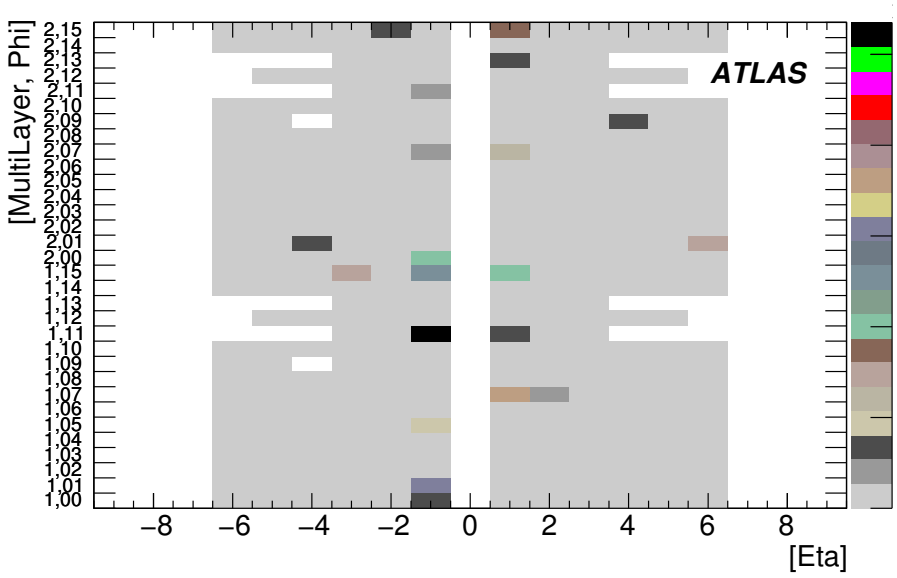

Figure 2: Multilayer hit-occupancy for the Barrel Middle MDT stations for run 91060. In the vertical scale the 16 phi sectors for multi-layers 1 (from 1.00 to 1.15) and 2 (from 2.00 to 2.15) are plotted while on the horizontal axis the 12 eta towers (from -6 to -1 for side C and from 1 to 6 for side A) are shown.

4.2 Barrel Trigger Chambers: RPC

Editor: Michele

During the cosmic runs 91060 data taken in autumn 2008 a few problems have limited the operation of RPC detectors. These problems can be summarized into four main categories: readout, trigger, gas and ambient temperature problems. The RPC readout is segmented into 64 trigger sector logics each one corresponding to about 6 trigger towers. Due to synchronization problems 11 of 64 sector logic boards were masked. Some other trigger towers were not operated because of broken optical links or fibers or because of initialization problems. A layer of an entire spectrometer sector of was turned off due to a broken gas line that prevented the proper flushing of the gas mixture inside the gas volumes. As a result of all these problems the trigger and readout coverage of the RPC during run 91060 was reduced to approximately 60%. In the left plot of Figure 3 a two-dimensional trigger distribution obtained requiring a 3 out of 4 majority coincidence in the low-p_T trigger boards for run 91060 is shown. During the winter shutdown a big effort has been done to fix the aforementioned problems, new firmware has solved the synchronization problems, optical links and fiber have been replaced as well as the gas lines. This made possible to reach, for rum 113860 collected in spring 2009, the 95% trigger coverage as shown in the right plot of Figure 3 .

Several studies on the trigger system performance were madeon run 91060. Trigger road implementation was checked. This consists in checking the spatial correlation between the *pivot* and the *confirm* strip involved in the lowp_T trigger: the *pivot* layers are the two more external layers, with respect to the interaction point, of a BM station while the confirm corrrespond to the more internal ones. In Figure 4 right RPC spatial correlation between pivot plane strip number and confirm plane strip number in phi view for a programmed trigger road obtained with cosmic muon is shown. The deviation from the 45 degrees correlation line is expected because of the relation between pointing tracks and phi-strip

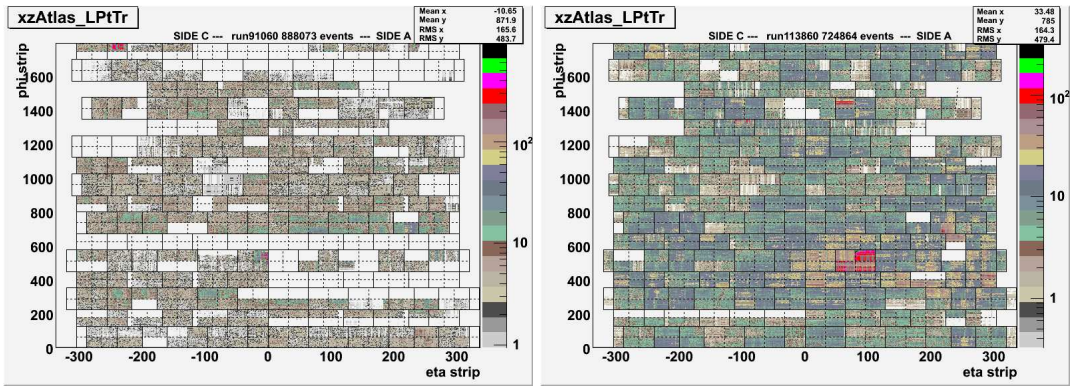

Figure 3: RPC Low-P$_T$ trigger coverage in the eta-phi plane for runs 91060, left, and 113860, right. Each eta and phi strip participating to a low-p_T correspond to an entry in this histogram.

geometry.

Noise studies were also performed, dedicated random trigger run were acquired and the single counting rate for each readout strip was measured. About 200 thousand strips were analyzed over a total of about 350 htaosand. In Figure 4 left the distribution of single channel noise counting rate per unit area measured with random triggers is shown. The noise is calculated by the total number of hits divided by the total number of random triggers and the readout window width of 200 ns and is normalized to the strip surface. Only a few hundred strips showed a single counting rate above 10 Hz/cm^2 that rate expacted to be prduced by the cavern background during high-luminosity LHC runs. The fraction of dead channel, only considering the part of the detector included in the readout during autumn 2008, was measured to be 1.5%, mainly due to front-end electronics problems which can be easily fixed.

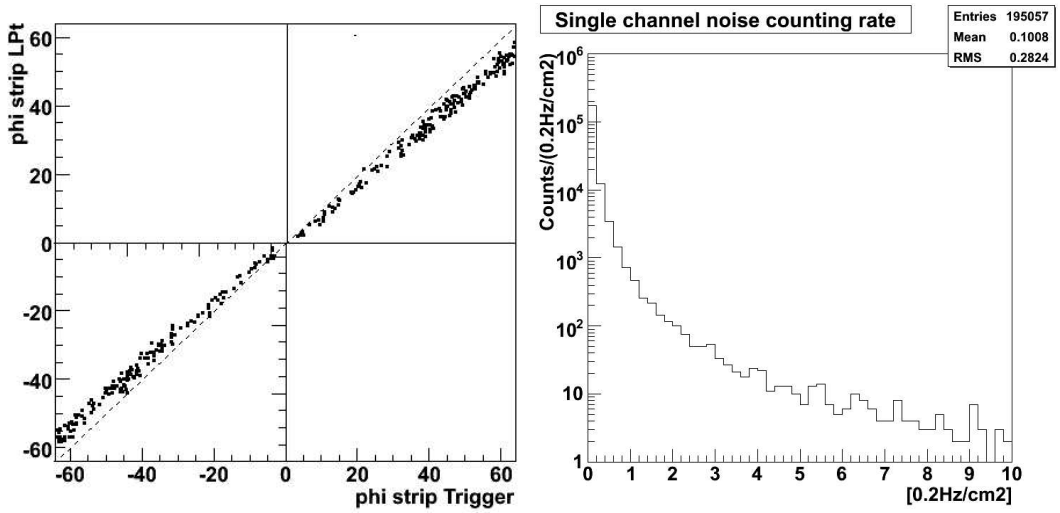

Figure 4: Right: RPC spatial correlation between pivot strip number and confirm strip number in phi view for a programmed trigger road in cosmics data. Left:RPC distribution of single channel noise counting rate per unit area measured with random triggers

4.3 End-Cap Trigger Chambers:TGC

In the end-cap the muon trigger is provided by the TGC chambers installed in three layers that surrounds the MDT end-cap Middle chambers. All together they form the so called ATLAS Big Wheels (BW). In addition TGC chambers are also installed in the innermost end-cap region (Small Wheels- SW) but they are only used to provide muon position and not for triggering. In the 2008 cosmic data taking, all the BW TGC sectors were readout. The inner stations of the TGC SW were the last to be installed in ATLAS and they were not fully operational during 2008 runs analyzed in this paper. For this reason they are not discussed in the following.

Two types of trigger coverage were adopted during fall 2008 data taking. One was optimized to study the end-cap muon detector system with cosmic rays. In this configuration all 12 TGC BW sectors were used to trigger. The other setting was optimized to provide the trigger to Inner Detector (ID) tracking sub-detectors. These data were used for timing adjustment of the ID. In order to mimic muons coming from the ATLAS IP only the five bottom sectors were used to trigger on that cosmic rays. The typical detector coverage in these two different trigger configurations is shown in Figures 5. There typical detector coverages are depicted by plotting coincidence positions in the XY plane for wire and strip hits for run 91060 (left) and run 91803 (right). The HV and front-end threshold setting, the gate widths for wire and strip and the trigger coverage for these two runs are listed in Table 3.

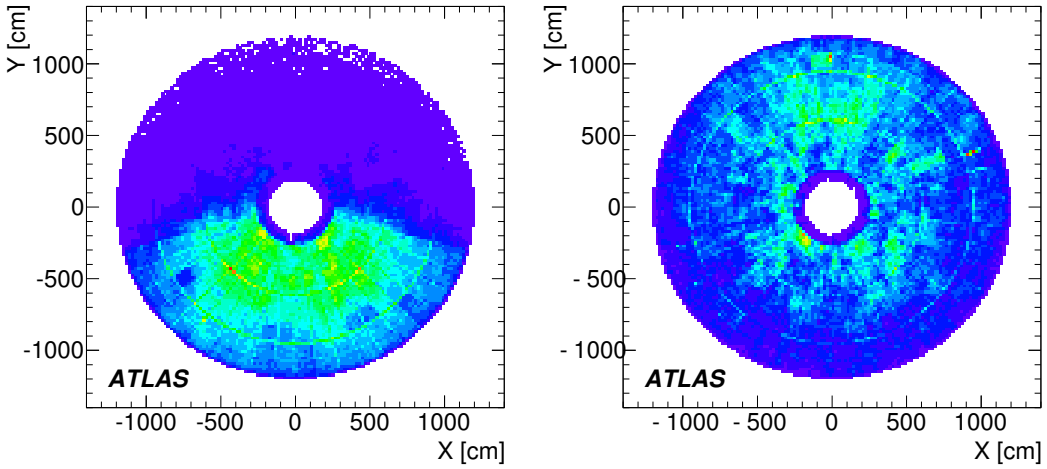

Figure 5: TGC detector coverage is shown by taking a coincidence of wire and strip hits. Left Figure shows that bottom 5 sectors (sector 8 to 12, $195^o < \theta < 345^o$) were used as trigger for timing scan for ID (run 91060) while right shows that all sectors were operated as trigger (run91803). Coincidences of wire and strip are also seen in non-trigger sectors (left) due to events triggered by RPC, cosmic shower or accidental noise.

Run	Trigger Sector	HV	Threshold	gate widths for wire / strip
91060	7 to 12	2800V	100mV	35ns / 45ns
91803	1 to 12	2650V	80mV	35ns / 45ns

Table 3: TGC Detector Coverage, high voltage, threshold and gate width.

For each trigger issued by the ATLAS Central Trigger Processor the TGC ROD sends to the data

acquisition system the data corresponding to three Bunch Crossings (Previous, Current and Next BC) contained into 2 separate buffers. Of the two buffers one is located in the front-end board (on detector) for wire/strip hit and low-P_T coincidence information. The other is located in the sector logic board (in the service counting room) for wire/strip high-P_T coincidence and trigger information. Each buffer has a programmable identifier that has to be be adjusted in order to read out the correct (Current) BC data. Figures 6 show readout timings for front-end and sector logic buffers for level-1 trigger issued by the TGC. About 98.6% of data in front-end buffer and 99.8% of data in sector logic buffer are read out with correct timing. The small populations in the previous or next BC are due to cosmic shower events or imperfect buffer depth determination.

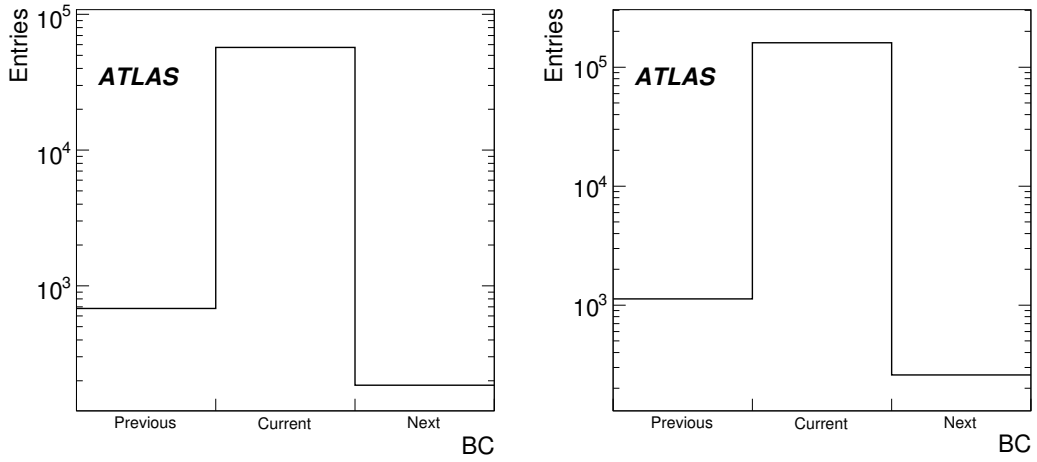

Figure 6: TGC front-end and sector logic depths are shown. Three BC crossing, previous, current and next are readout.

At the beginning of the 2008 cosmic data taking, 28 chambers out of 3588 were not functional due to several failures (i.e., damaged chambers, control cables, power supplies, ...). Most of them were replaced or recovered by HV training with pure CO_2. After the repairing work still 262 channels in three chambers remained dead. For two chambers the nominal HV could not be applied even after the HV training, and the remaining one, which is located in the SW (inner station) and is not used for triggering, was mechanically broken by an overpressure accident. In addition there were 30 single dead channels and 285 dead channels due to 18 problematic ASD (Amplifier-Shaper-Discriminator) chips. Due to noise, corresponding to an occupancy of greater than 2.5%, additional 128 channels were masked off to avoid large data size and possible fake triggers for coming physics runs. To summarize in the fall 2008 cosmic ray run the total amount of dead and masked channel was of 705 out of about 318k corresponding to a fraction of about 0.22%. None of the dead and masked channels caused a hole in the trigger acceptance thanks to the coincidence trigger logic redundancy (3 out of 4 and 2 out of 3 majority requirements for low-P_T and high-P_T triggers).

5 Precision Chambers calibration

5.1 Calibration procedures

The muon precision chambers requires a calibration procedure in order to convert the measured drift times into drift distances from the anode wire (drift radius) that are subsequently used into patter recog-

nition and track fit procedures. The calibration of the MDT chambers is performed in three steps using the acquired data: In the first step the drift-time measurements of the individual chambers are time aligned (t_0 determination), in the second step the space drift-time relationships ($r(t)$ relations) are determined, in the third step the spatial resolutions of the drift tubes are measured. The calibration constants determined as described in the following are then loaded in the ATLAS conditions Data Base (COOL) and retrieved, using an Interval Of Validity (IOV) mechanisms, during the muon data offline reconstructions.

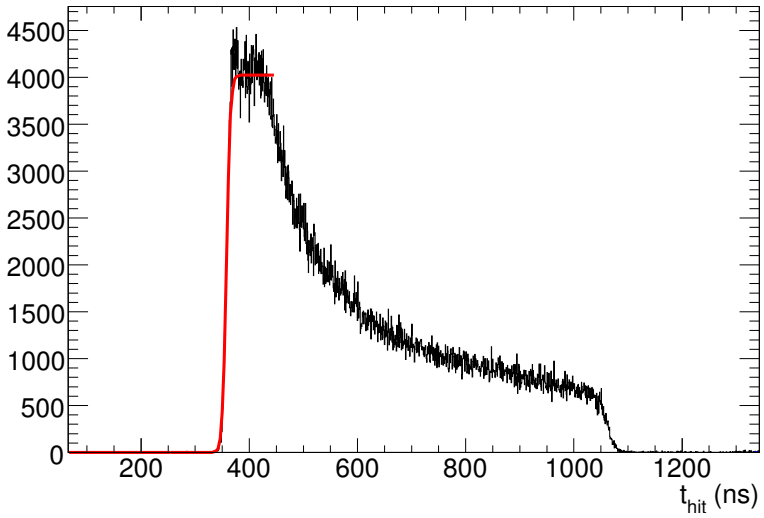

Figure 7: Typical time spectrum of hits from comsic ray events of an MDT chamber. The position of the leading edge of the spectrum, t_0, is determined by fitting a Fermi function (shown in red) to the beginning of the spectrum.

The t_0 value represents a time offset that is needed to convert the measured time into the real electron drift times associated to the muon drift distance from the MDT wire. In LHC collissions this offset depends on many fixed delays like cable lengths, FE electronics response, LV1 trigger latency, time of flights of the muons from the ATLAS interaction point and it has to be determined for each drift tube. They are btained by fitting Fermi step functions to the leading edges of the drift time spectra as depicted in Figure 7. The achieved precision expected in LHC collisions depends on the available statistics: less than 1 ns statistical error can be achieved with about 10k muons crossing the analyzed drift tube. The statistical uncertainty of the t_0s of $\leq$1 ns does not significantly degrade the drift time resolution of the chambers which is of the order of 5 ns.

As the MDT chambers are operated at different temperatures depending on their positions in the muon spectrometer, the space to drift-time relationships $r(t)$ of the chambers differ from each other and are determined separately. In addition to temperature effects also large variation of the magnetic field inside the muon spectrometer causes different $r(t)$ relations (Lorentz angle effect). An initial rough estimate of $r(t)$ is obtained with an accuracy of 0.5 mm by integrating the drift-time spectrum of a chamber. This procedure is correct under the approximation of a uniform dn/dr distribution as shown in following equation:

$$\frac{dn}{dt} = \frac{dn}{dr}\frac{dr}{dt} \approx \frac{N_{hits}}{r_{max}}\frac{dr}{dt} \Rightarrow r(t) \approx \frac{r_{max}}{N_{hits}} \int_0^t \frac{dn}{dt'} dt'.$$

Due to the δ-ray electrons and other effects this approximation is good at the few hundred μm level. An $r(t)$ relationship with an higher accuracy, of about 20 μm, is obtained from the initial estimate by

applying iterative corrections $\delta r(t)$ which minimize the residuals of track segments fitted to the hits of chambers. The adopted minimization procedure, the so-called *auto-calibration procedure*, takes into account the dependence of the parameters of the fitted segment on the applied corrections $\delta r(t)$ and is mainly based on geometrical constraints coming from the precise knowledge of the wire positions. Figure 8 shows a typical residual distribution of a chamber after the auto-calibration procedure as a function of the distance of the reconstructed track segment from the hit anode wires.

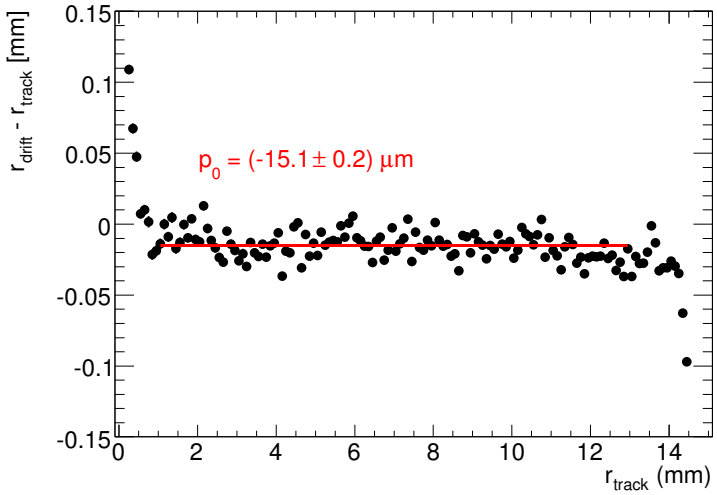

Figure 8: Track segment residuals in an MDT chamber as a function of the track impact radius after the $r(t)$ calibration.

In cosmic ray events several additional sources of time jitters are spoiling the MDT drift measurement perfromance. The first source of time jitter is the due to the fact that cosmic muons are crossing the tubes with an arbitrary phase with respect to the Front-End electronics clock (corresponding to the LHC distributed clock). In LHC collisions the FE electronics is synchronous with the LHC Bunch Crossing (BC): the phase between the clock and the recorded hit is at fixed delay that is absorbed in the t_0 definition. For the cosmic events this implies an additional time jitter corresponding to a 25ns uniform distribution. An additional source of time jitter during the cosmic rays runs analyzed in this paper is relayed to the time spread between the different Barrel trigger towers as described in Section 3. From the MDT drift-time spectra only an average values of t_0 per tube can thus be obtained. Two diferent methods has been used to reduce the impact of these effect on MDT performance: the *RPC-time correction* and the MDT t_0-*refit*. The details and the achieved performance for both procedures are detailed in Section 6.1. In the following a brief description is given.

The RPC-time correction consists in using, event by event, the trigger time as measured by the RPC chambers. These time corrections has been applied only to a fraction of the barrel chambers: the Barrel Middle stations. These chambers are physically coupled to the RPC stations used to issue the cosmic trigger. The extention to other station types would require a more complex algortihm that should be able to make ad-hoc corrections depending on which RPC trigger tower has issued the trigger for the analyzed event. They cannot be applied to the end-cap region since the TGC do not provide a measurement of the tirgger time but only select the appropriate BC. The previously shown results are obtained subtracting the time measured in a RPC-chamber from the trigger time. With this correction the additional time jitters mentioned above, which are of the order of 100 ns, are strongly reduced to the few ns level as shown in Section 6.1.

The alternative procedure that has been used to reduce the time jitter effects mentioned above, the

t_0-refit, consists into adding to the segment fit procedure an additional free parameter corresponding to a global, event-by-event, time offset. In addition to the standard segment parameters a time offset is applied to all the hits involved into the segment. In addition to reduce the single tube resolution, as discussed in Section 6.1, this has also an impact on the precision of the auto-calibration. As can be seen in Figure 9 where a precision of the order of 50 μm is obtained.

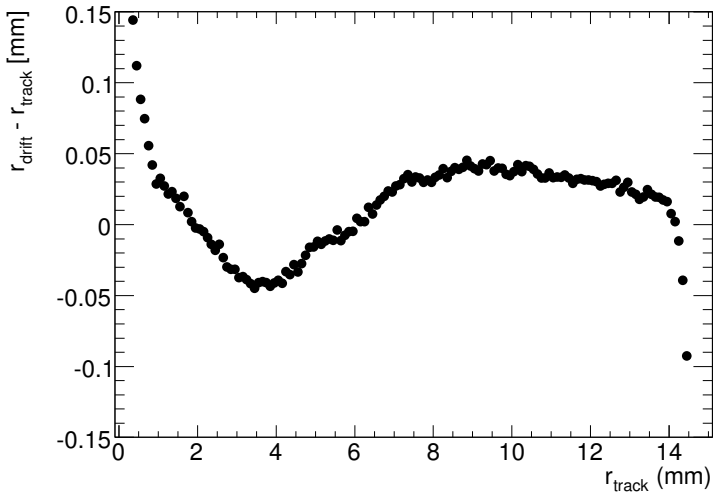

Figure 9: Track segment residuals in an MDT chamber as a function of the track impact radius after the $r(t)$ calibration using the t_0-refit procedure.

5.2 End-cap chambers $r(t)$ from Monitoring chamber

For the end-cap MDT, due to limited cosmic ray statistics, a different method to determine the $r(t)$ relations has been used. A global $r(t)$ has been derived from a gas monitoring chamber, a small MDT chamber located on the surface which monitors gas input and output to the ATLAS MDT system [9]. This chamber benefits of a very large cosmic ray rate and can therefore determine $r(t)$ functions with high precision in a short time intervals. The cosmic muons are triggered by scintillators mounted on the monitoring chamber. The trigger time is measured and subtructed to the tube drift times: in this way the time jitter related to the FE clock synchronization with cosmic events is removed. Cosmic data from the monitoring chamber is used to derive a drift function every 6 hours and thus monitor the ATLAS gas properties. Figure 10 shows the variation of the maximum drift time (time corresponding to muons crossing the dirft tube close to its edge) over the 2008 September-October period. Two $r(t)$ functions were used to cover the fall 2008 run period, one from for the period corresponding to run ranging from number 87760 to 90270. A second $r(t)$ was used for the remaining 2008 running period. For each run period the $r(t)$ functions were modified to account for the chamber temperature using data from temperature sensors mounted on each MDT. The temperature corrections to the $r(t)$ were derived from the Garfield simulation program [10]. From top to bottom of ATLAS temperature varies by about 4^o C, resulting in a change in maximum drift time of about 10 ns.

Figure 11 shows the distributions of the average fit residuals from track segments in all end-cap chambers from run 91060. A Guassina fit is superimposed. The gas monitor $r(t)$ works very well with an average residuals standard deviation of about 100 μm and few outliers.

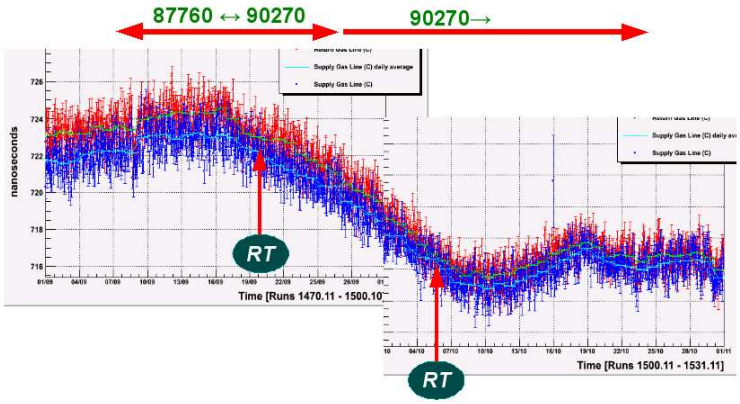

Figure 10: The maximum drift-time that was measured by the gas monitor chamber versus the time

6 Detector Performance: single hit efficiency and resolution

6.1 MDT

In this section the cosmic ray collected in the ATLAS cavern are used to measure the MDT performance. Several aspect related to cosmic rays have been taken into account since they have a large impact on the measured performance. In particular the asyncronous behaviuor of cosmic ray muons with respect to the LHC clock as required the development of dedicated techniques as explained in teh following subsections.

6.1.1 MDT Drift Time Spectra and t_0-refit

The analysis of drift time distribution of individual tubes is an important aspect of MDT performance. The minimum, t_0, and maximum, t_{max}, drift times correspond to particles passing very close to the wire and to the tube walls, respectively. The number of hits recorded in a small time window before the t_0 can

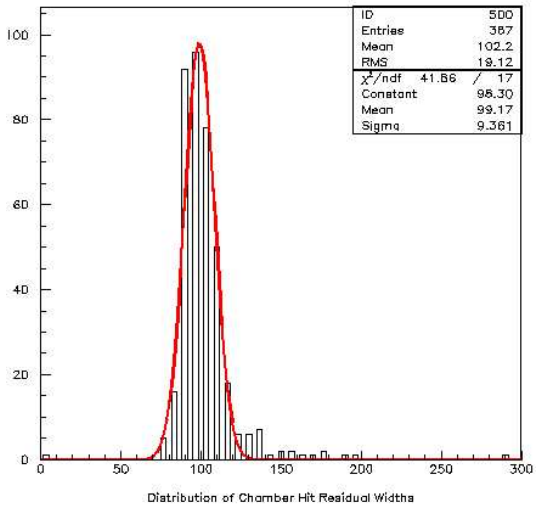

Figure 11: Residual distribution obtained with the gas monitor rt.

be used to estimate the level of noise and of cavern background (that will be present in LHC collisions). A precise knowledge of the t_0 for each tube is essential for high quality segment and track reconstruction. As explained in Section 5 , for cosmic rays some additional time jitters are present and must be accounted for. In order to improve the quality of track reconstruction, a modified segment fitting algorithm has been implemented accounting for a global time offset, per event, as an additional parameter to the segment fit [8], referred to as t_0-refit. The performance of the t_0-refit algorithm has been investigated in the past both using simulated data and data taken with a BIL (Barrel Inner Large) chamber in a cosmic rays test stand in controlled trigger conditions [8]. The achieved t_0 resolution ranged between 2 and 4 ns depending on the chamber geometry (8 layer chambers have better resolution then 6 layer chambers) and the hit topology (e.g., it is not possible to determined the t0 if all hits are on one side of the wire). To select good quality segments a minimum of 5 MDT hits is required in the following studies and segments with all hits passing on the same side of the wires are removed.

In addition to the t_0-refit also the RPC-time correction method has been used for MDT chambers geometrically coupled with RPC trigger chambers. This is the case of Barrel Middle chambers where the time measured by the adjacent RPC chambers can be used to correct for global time offset and additional time jitters as describer in Section 5.

An example of the effectiveness of the method is reported in Figure 7 where the time spectra for one BML chamber is shown after RPC timing corrections. The steepness of the rising edge is definitely improved, passing from 22 ns from the spectrum without RPC timing corrections, to 3 ns, a value in agreement with test beam data. The precision on the RPC-time correction has been estimated to be of the order of 2 ns as explained in Section 6.2. This also includes the contribution of the signal propagation time on RPC phi strips.

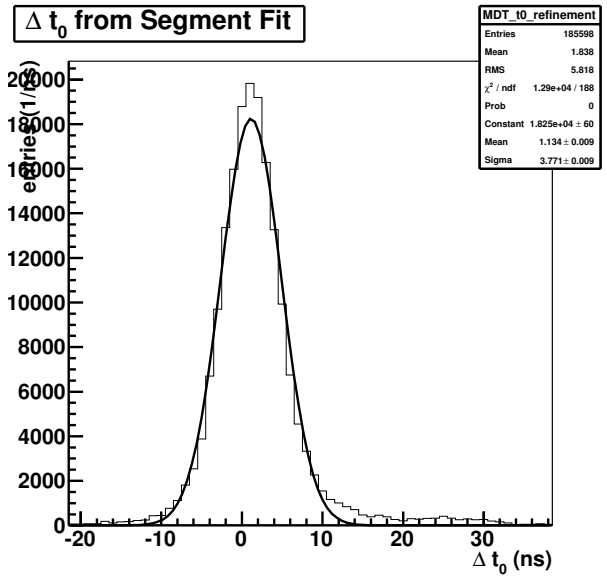

Figure 12: t_0 free parameter distribution obtained from the t_0-refit method on segments where RPC-timing corrections were applied. The width of the distribution is a convolution of the time uncertainties of the RPC-timing correction and the t_0 refit method. FIGURE MUST BE REDONE

Segments can thus be reconstructed in two ways: using the RPC timing correction with a fixed t_0, or ignoring RPC timing corrections and using the t_0-refit method. The spread in the differences between the fitted t_0 and the RPC timing correction per segment for one BML chamber is shown in Figure 12. The measured standard deviation of about 4 ns is consistent with an uncertainty of about 2 ns from the

RPC timing correction added to another of about 3 ns introduced by the t_0-refit method. Tails up to 30 nsec are present in the distribution due to bad hit-topologies and background hits.

6.1.2 Single-hit Spatial Resolution

The single MDT tube spatial resolution as a function of the drift distance can be studied on chambers for which the segment reconstruction with the RPC timing corrections is applied. As an example one BML chamber (BML2A03, position 2 in eta, side A, 3rd sector in phi) has been chosen.

The method is based on an iterative procedure. At first iteration an approximate input resolution function is assumed. Segments with a minimum of 6 hits are considered. These segments are fitted again after removing one hit at the time and the distribution of the residuals for the excluded hits is computed as a function of the drift distance from the wire. The widths of the residual distribution ($\sigma_{resid}(r)$) is measured as a function of the drift distance. The errors on straight line fit (depending on the assumed tube resolution) are then propagated to the selected hit ($\sigma_{SL}(r)$). The resolution is then computed by quadratically subtracting from the standard deviation of the residuals the extrapolation error due to the fit:

$$\sigma_{resol}(r) = \sqrt{\sigma_{resid}(r)^2 - \sigma_{SL}(r)^2} \tag{1}$$

The procedure is iterated using the new resolution function until the input and output resolutions agree within statistical errors; a small number of iterations (two to four) is usually needed.

In Figure 13 the tube resolution from cosmic data on the chamber BML2A03 is shown as the green error band. The width of the band accounts for the systematic uncertainty of the method. Also reported is the resolution curve obtained on an MDT chamber from the high energy muon test-beam [4, 5] with well controlled trigger timing. This can be considered as a reference curve for single-hit resolution performance. The resolution measured with cosmic data is consistent with a time degradation of the reference curve of about 3 ns, in reasonable agreement with the 2 ns time resolution already quoted for the RPC timing corrections, in addition to minor effects, among which, multiple scattering and individual tubes differences in t_0.

An alternative method to determine single-hit space resolution, based on segments reconstructed with the t_0-refit method and without RPC timing corrections, has been applied on the same chamber. This method also relies on an iterative procedure: the initial resolution $\sigma_{resol}(r)$ is parametrized by a smooth function. Using this parametrization the pull of a selected MDT tube is determined by fitting a straight line to all the hits with the exception of the hit under study (selected hit). The errors on straight line fit are then propagated to the selected hit ($\sigma_{SL}(r)$). The total error on the residual is than calculated as: $\sigma_{resid}(r) = \sqrt{\sigma_{resol}(r)^2 + \sigma_{SL}(r)^2}$ The pull is then defined as the residual of the MDT hit divided by the total error (σ_{resid}). This procedure is iterated until the pull distribution has a standard deviation of 1. The obtained resolution is also reported as a dashed line in Figure 13. The uncertainty on this method is estimated to be of about 5% and it is consistent with an additional time uncertainty of about 3 ns introduced by the t_0-refit method.

6.1.3 Tube efficiency

The single tube efficiency was studied by reconstructing segments in the chamber with all tubes but the one under observation (i.e., by excluding one MDT layer at the time in segment reconstruction). Two different types of inefficiencies may occur: *i)* absence of hits in the tube; *ii)* a hit is present in the tube but is not associated to the segment because being at at a distance larger that the defined cut. Inefficiencies of type *i)*, referred to as *hardware inefficiencies*, are expected to be very small, mostly contributing at large drift distances, near the tube walls, where the short track length results in fewer primary electrons.

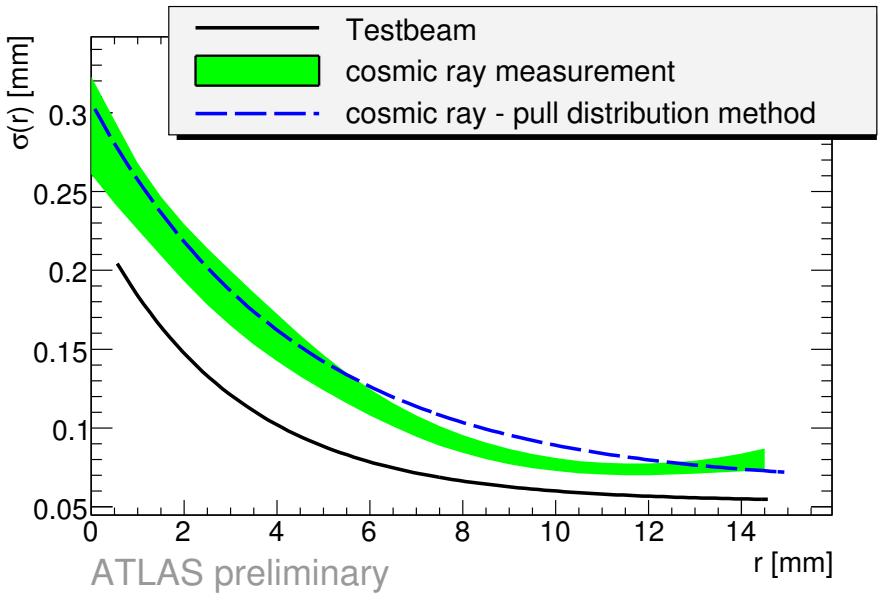

Figure 13: MDT tube resolution as a function of the radius. The green band and the dashed lines represent the resolution measured on cosmic ray samples with the two differnt methods described in the text. The dashed line represent the resolution measured in previous test beam.

Inefficiencies of type *ii)*, referred to as *tracking inefficiencies*, are dominated by $\delta-$electrons, produced by the incoming muon, which can mask the muon hit if the $\delta-$electorn has smaller impact parameter than the muon. The tube noise can be an additional source of this type of inefficiency.

Figure 6.1.3 shows the signed residual for the hits of the tubes under observation for one Barrel chamber, BML2A03, as a function of the distance of the muon segment from the wire. A large population at small residuals, compatible with the residuals resolution, is visible. Large positive residuals are associated with early hits mainly due to $\delta-$electrons. In the case the hit is not found in the tube traversed by the track (thus a residual cannot be computed) a residual of 15.5 mm is assigned, larger then the tube radius. This contribution, related to hardware inefficiency, is visible at the top of the plot and it peaks close to the tube wall as expected.

The tracking inefficiency is defined has the fraction of hits with a residual from the segment that is larger than n times its error, this being a convolution of the tube resolution and the track extrapolation error. Figure 6.1.3 shows the hardware efficiency as well as the tracking efficiencies as a function of the drift distance for values of n=3, 5, 10. Integrated tube efficiencies are also reported in the legend. Efficiencies decreases with increasing radius, mainly due to the contribution of δ electrons, whose expected contribution to tracking efficiency is in the range between 3 to 5%. The hardware inefficiency is negligible being only relevant very close to the tube wall.

In Figure 6.1.3 the integrated efficiencies for each tube of the BML2A07 chamber is reported for n=5. The average efficiency is of about 96%. Efficiencies consistent with zero have been obtained for two tubes with disconnected wires as can be seen in the expanded view on the right plot. Those tubes were not considered in the estimate of the average. Tubes with efficiencies lower than 90% are detected at the edges of the chamber layers due to low statistics, accounted for by the large statistical errors.

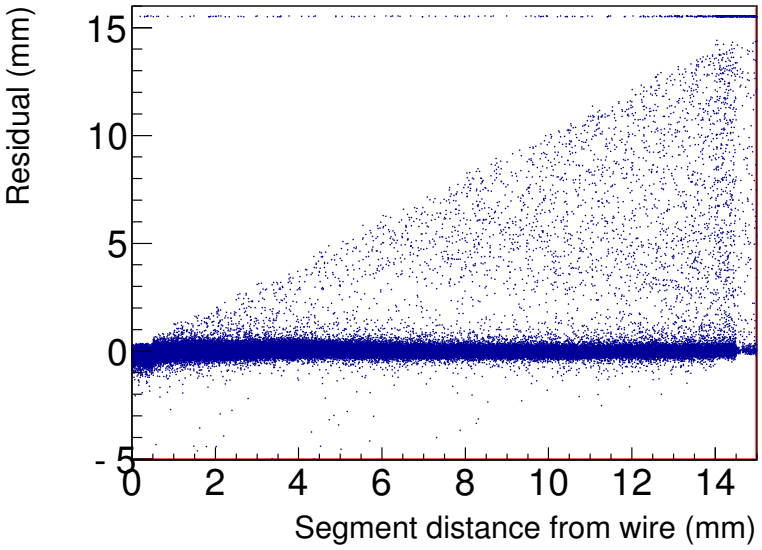

Figure 14: MDT hit residuals for tubes excluded by the segment fit but expected to be crossed by the muon as a function of the distance of the track from the wire. Small residuals are associated with efficient hits. The triangular region is dominated by early hits coming from $\delta-$electrons. Missing hits are assigned at residuals equal to 15.5 mm as expained in the text.

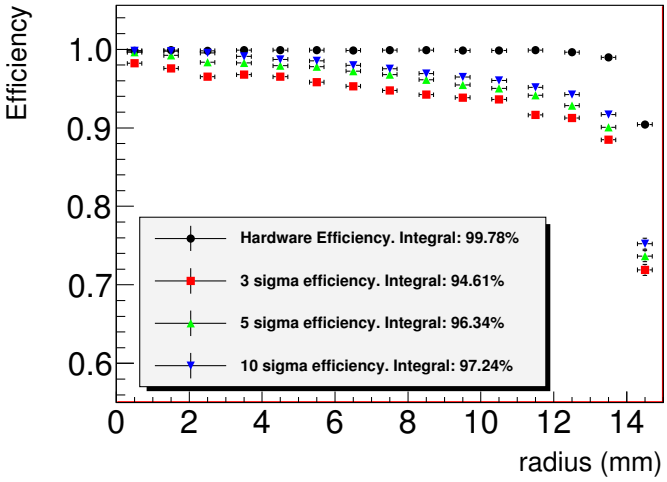

Figure 15: Tube efficiency as a function of the drift distance averaged over all tubes of the chamber BML2A03. Reported are the hardware efficiency, as well as tracking efficiencies for hit residuals smaller than 3, 5, 10 times the estimated residual standard deviation.

6.2 RPC

In addition of providing muon triggers the RPC detector is also expected to identify the Bunch Crossing (BC) at which the muon was produced. This requires an intrinsic time resolution that is much better than

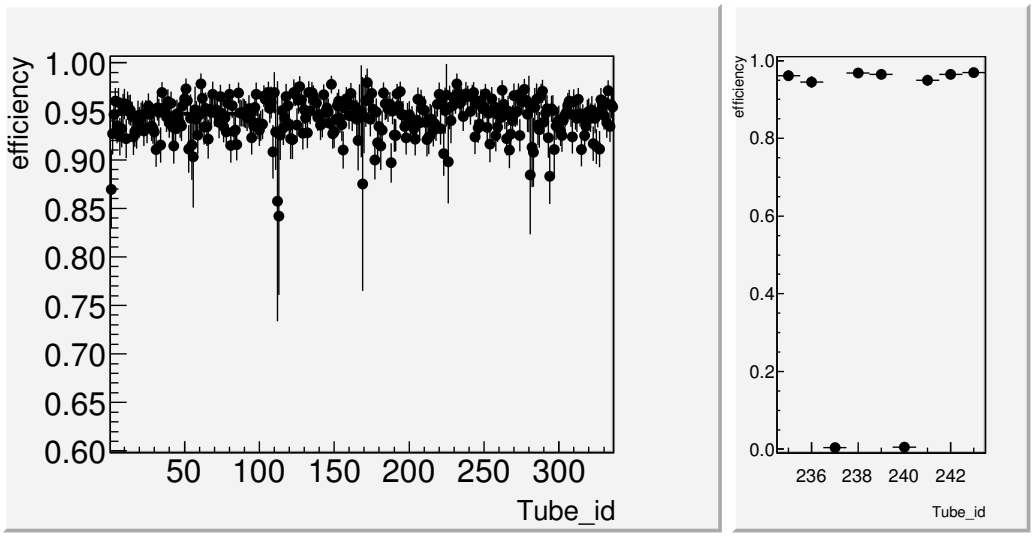

Figure 16: MDT single-tube efficiencies with n=5 cut, as explained in the text, for the chamber BML2A07. The right plot shows an expanded view in the region where two disconnected tubes were found with tracking efficiency consistent with zero.

the time difference btween two consecutive LHC bunches corresponding to 25ns (40 MHz clock). The RPC time resolution has been measured from the time difference distribution of the two adiacent layers of the BM pivot plane in the non-bending view. This method allow the measurement of the RPC time resolution without correcting for the muon time of flight and signal propagation along readout strip. The result is shown in Figure 17. From this plot a time resolution of about 1.8 ns is derived corresponding to the fitted standard deviation divided by $\sqrt{(}2)$. In this measurement only hits associated to reconstructed muon tracks and belonging to events with one and only one RPC trigger are considered.

Two other important RPC quantities that are related to the detector working point are the read-out panel efficiency and the spatial resolution as a function. This last quantity is very sensitive to the hit *cluster size* that is defined as the number of adjacent hits produced by the crossing muon.

In order to determine the RPC efficiency two main issues have to be taken into account: first, RPC detectors are actually providing the muon trigger (*trigger bias*) and, second, they are also used in track reconstruction; in particular, they are the only source of space measurements in the non-bending direction. The second effect is expected to have negligible contribution to the efficiency measured in the bending plane where track recostruction is driven by the precision chambers (MDT) hits. The distribution of average efficiency for RPC Barrel Middle chambers readout panels in run 91060 is shown in Figure 18. The reconstructed track is extrapolated to the RPC plane, and a panel is defined to be efficient if it has a hit within a $\pm$70mm window. The tail at lower efficiencies is due to known problems, which were mostly fixed in subsequent runs.
In order to check the impact of the trigger bias the same measurement has been applied to a sample of cosmic events triggered by the calorimeters (*LV1Calo* trigger). This sample is unbiased with respect to the RPC trigger. The result is superimposed in Figure 18 and a good agreement with the result obtained with the same method on RPC-triggered events is abserved.

The spatial resolution is strongly reated to the cluster size of hits associated to a muon track. In fact for events of cluster size 1 a spatial resolution of about the strip pitch diveded by $\sqrt{12}$ is expected. For events with cluster size 2 a better resolution is expected since this is possible only for muons crossing a small region in between two adiacent strips. The spatial resolutions as measured on eta (bending

coordinate) readout panels, for clusters of size 1 and 2 is shown in Figure 19. The residual distributions are fitted with a Gaussian function, and the resulting standard deviation is divided by the strip pitch, to allow comparison between different panels. As expected, clusters of size 2 give an improved spatial resolution.

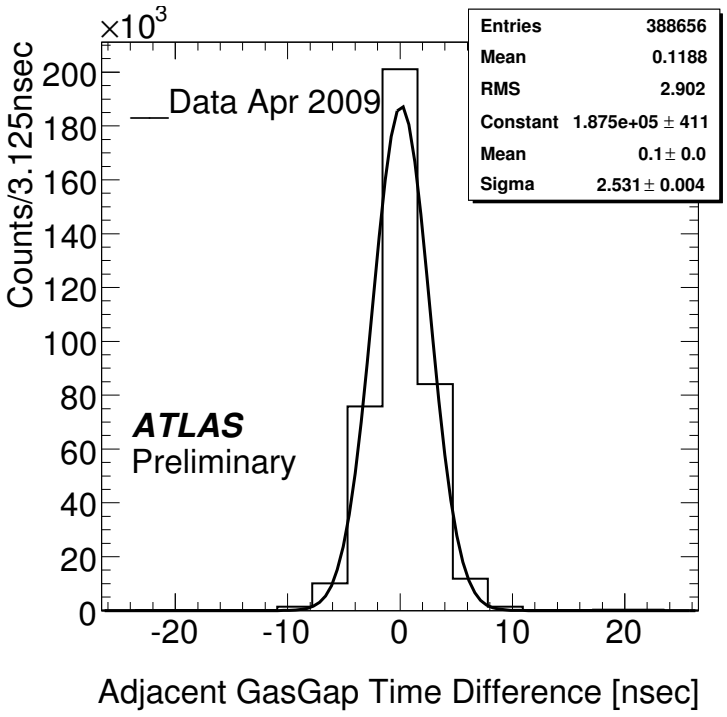

Figure 17: Distribution of the relative time between the two RPC layers in the non-bending view pivot plane.

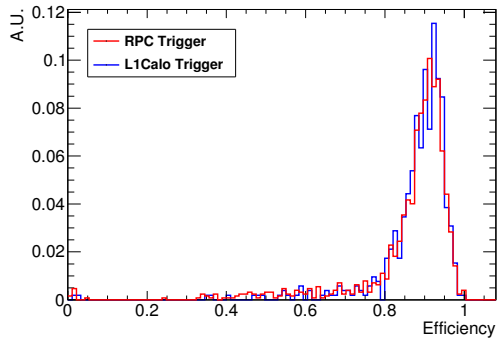

Figure 18: Distribution of average efficiency for RPC of BM panels for run 91060. The two histograms are referred to two different trigger sources: RPC trigger and calorimeter-based trigger (L1Calo). The histograms are normalized to unity.

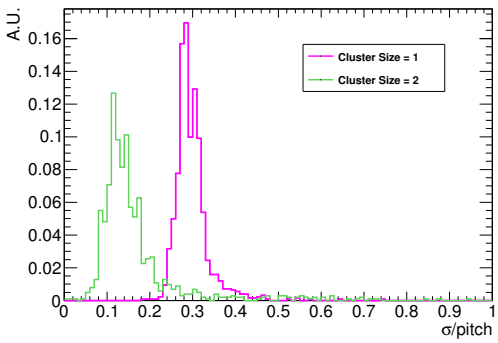

Figure 19: Distribution of spatial resolution for η RPC panels. Only BM chambers are shown. Spatial resolution is divided by the strip pitch, and histograms are normalized to unity.

6.3 TGC

The efficiency is an essential parameter for the commissioning of TGC toward beam collisions. Cosmic data has been used to measure this quantity. The TGC detector is expected to have a wire efficiency of more than 98% in the active region. Depending on the chamber type the inactive regions due to the support structures (wire support and the button supports) are expected to cover an area in the range 3.4% to 6.0%. This implies that the overall chamber efficiency per layer is expected to be in the range 92% ro 95% depending on chamber type. In order to optimize the trigger efficiency these inactive regions are designed to be staggered with respect to the trajectories of high momentum muons coming from the ATLAS interaction point. The trigger coincidence majority is defined such that the trigger efficiency is not affected by the support structures. In the cosmic run 91060 the trigger majority was defined as 3 out of 4 layers in the 2 TGC doublet chambers (referred to as TGC2 and TGC3), as described in Sections 3 and 4.3.

To evaluate the wire efficiency with the cosmic muons, the following differences with respect to the collision events should be handled; the random arrival timing of the cosmic muons with respect to the LHC clock, the trigger bias since events triggered by the TGC are used to determine the TGC wire efficiency, the presence of cosmic shower events with high multiplicity, the non pointing trajectories of the cosmic muons. In order to overcome the above mentioned problems, the wire efficiency has been evaluated with muon tracks selected by applying the following criteria. To evaluate the efficiency of a layer in the doublet chamber, a hit in each of the other three layers is required. These three hits must be associated to the current Bunch Crossing (BC). This requirement limit possible ineffiency due to random phase of cosmic muons with respect to LHC clock. The requirement of only one wire hit per layer also removes the high multiplicity events due to the cosmic showers. As the result of this selection, the 3 out of 4 trigger condition is satisfied independently of the presence or not of a hit in the layer under evaluation. The efficiency per layer is thus determined in an unbiased way. Similarly for the triplet chambers (3 layers TGC used in high-P_t trigger, referred to as TGC1), it is required that the two layers which are not under evaluation satisfy the condition of the 2 out of 3 layer coincidence. To remove the background events, a reconstructed segment passing within the hit wire areas is required. All muon tracks passing the selection criteria described above are used to get the number of the expected hits in the layer under the test. The fraction of the measured hits in any BC (previous, current and next) in the tested layer with respect to the number of expected ones is defined as the hit efficiency of that layer.

Figure 20 left and Figure 20 right show the 2-D mapping of the efficiency in the wire-strip plane and the projection of the efficiency to the strip channels, respectively, for the layer 5 of a TGC chamber of type T7. The inactive regions due to the wire supports can be clearly seen as expected based on the TGC design (the bands in Figure 20 right). Figure 21 left shows the TGC wire efficiency for only active regions as a function of the high voltage. Due to the limited statistics, only TGC of type T7, T8, and T9 are used in this analysis. The result from the 2008 combined run (circle in the Figure 21 left) agrees with the results from the beam test on the surface at CERN in 2003 (square in the Figure 21 left) within 1% level, which can be explained by the difference of the threshold voltage. Figure 21 right shows the overall TGC wire efficiency including the support structures as a function of the high voltage.

Overall efficiency including the support materials inside the chambers are evaluated. In this analysis, all types of chambers are included. The extrapolated muon track is required to cross the layer under evaluation at list 10cm away from its edges. Figure 22 shows the distributions of the wire efficiency at the different high voltage values, 2650, 2750, 2800 and 2850 V. The mean value of the efficiency at the nominal voltage of 2800V is found to be of about 92% as expected once inactive-region contributions is taken into account.

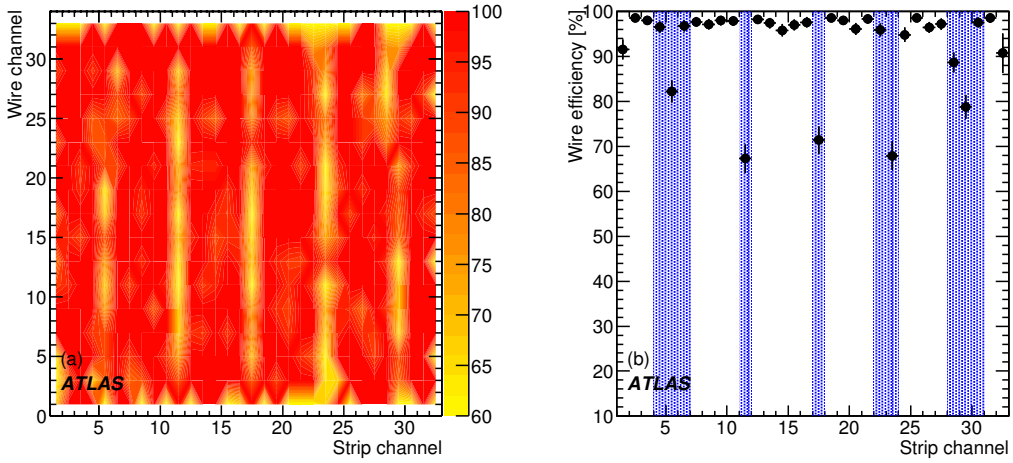

Figure 20: Left efficiency map for layer 5 of a TGC chamber (this specific case chamber of type T7). The horizontal axis is the strip channel and the vertical axis is the wire channel. Right efficiency projection to the strip channels. Channels within bands include wire support structure in its channel. Observed efficiency drops are consistent with the wire support locations.

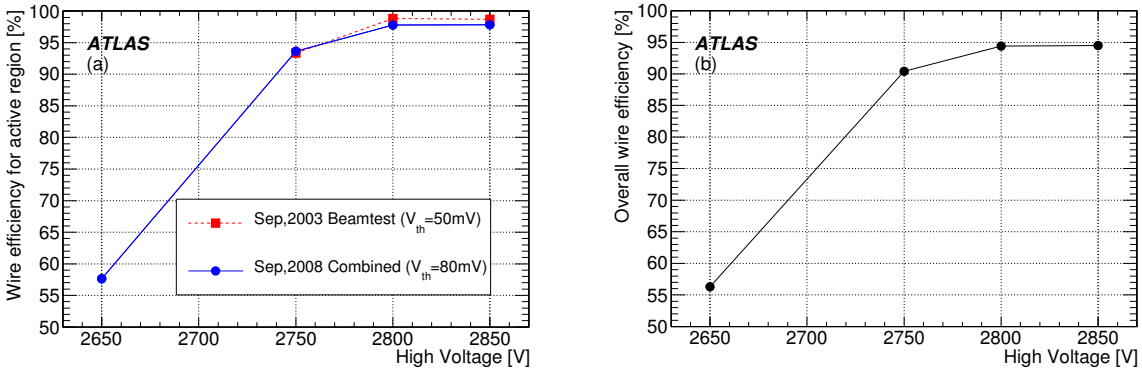

Figure 21: Left TGC wire efficiency as a function of high voltage for active regions only. Circle dots show the combined run result in 2008, while square dots show the test-beam results achieved in 2003. The difference of altitude (80m) is taken into account. Both results are consistent within 1%. Right TGC wire efficiency including the wire support structures as a function of the high voltage.

7 Precision chamber alignment

The ATLAS muon spectrometer employs an air-core toroidal magnetic field, which has the advantage of causing only minimal multiple scattering due to the small amount of material present between chambers. A consequence of this design is the relatively low magnetic field strength that can be reached: the bending of a 1 TeV muon track in the magnetic field is such that the track sagitta varies between 0.5 mm at pseudorapidity $\eta = 0$ and 1 mm at $\eta = 2$. Consequently, in order to measure the momentum of a 1 TeV muon to 10% at all angles, the error on the sagitta measurement must be less than 50 μm in the bending direction of the magnetic field, transverse to the MDT tubes and wires. Muon tracks are detected in three about equally spaced layers of chambers. The intrinsic resolution of the MDTs results in a sagitta error of about 50 μm, and the additional error from the chamber alignment should be smaller than that

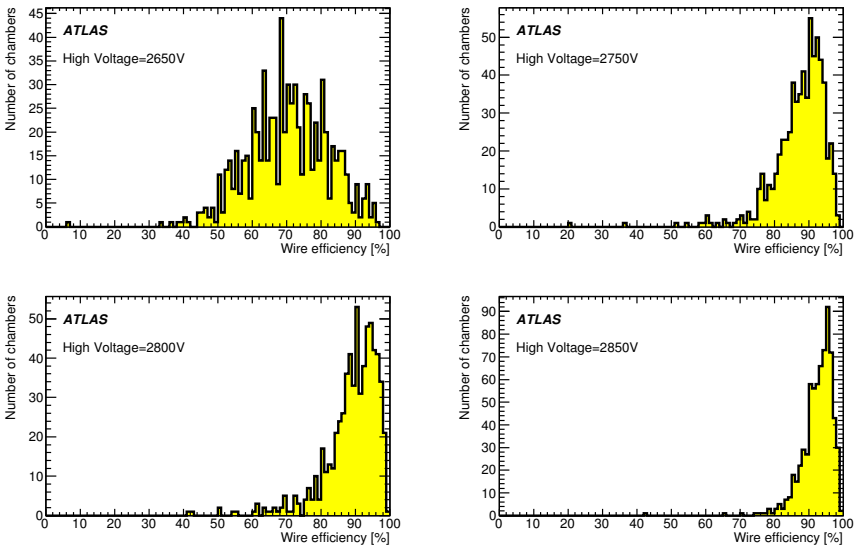

Figure 22: The distributions of TGC wire efficiency per layer of individual chambers at different high voltage values, 2650, 2750, 2800 and 2850 V. The result at 2800V, which was the nominal voltage in 2008, is obtained with run 91060, while other results are obtained with other runs.

value. As long-term mechanical stability in a large structure such as ATLAS cannot be guaranteed at this level, a continuously running alignment monitoring system [11, 12] is required in order to fully exploit the intrinsic resolution of the spectrometer. This system is based on optical and temperature sensors, and is designed to detect slow chamber displacements, occurring at a timescale of hours or more. The information from the alignment system is used in the offline track reconstruction to correct for the chamber misalignment – no physical adjustments are made to the chamber positions after the initial positioning.

There is a large variety of optical sensors in the alignment system, all sharing the same principle: a source of light is imaged through a lens onto an electronic image sensor acting as a screen. The source of light is either a back-illuminated coded chessboard pattern (RASNIK mask), or one or several pairs of point-like light sources (BCAM and SaCam systems). In addition to optical position measurements it is also vital to determine the thermal expansion of chambers, by measuring their temperature. In total, there are about 12000 optical sensors and a similar number of temperature sensors in the system. They are mounted on chambers and on auxiliary reference objects, forming a complex network, the layout of which was validated and optimized by Monte-Carlo simulations. During ATLAS running, sensor data are acquired in a combination of sequential and parallel operations. Images are analyzed on-line, and only the analysis result (i.e. the spot position for BCAM and SaCam images, and the decoded position of the mask for RASNIKs) plus some diagnostic information is stored in a database, yielding a data volume of about 0.1 KB per image. Some fraction of the raw images, having a size of about 100 KB each, is retained for debugging purposes. One readout cycle, yielding one image from each sensor, takes about 30–60 minutes. The alignment data acquisition is integrated with the ATLAS detector control system.

Optical and temperature sensors are calibrated, so that they can be used to make *absolute* measurements of muon chamber positions in space, rather than only following their movements with time, relative to some initial positions. The expected accuracy of this initial calibration differs between the barrel and the end-cap systems as expalined in the following. In the end-cap is possible to determine the spectrometer alignment at the desired accuracy without making any use of muon tracks, and straight tracks from runs without magnetic field can instead be used for independent cross-checks of the optical

system. This is quite important, given the stringent accuracy requirement and the large number of systematic effects that need to be kept under control. Calibrating alignment sensors at the required level of accuracy (typically around 20 μm for positions and 50 μrad for rotations) was performed by a series of measurements on a calibration stand, the geometry of which is accurately known e.g. from measurements with a coordinate-measuring machine. Sensor mounts on chambers and on auxiliary objects also have to be calibrated. In total, there are of the order of 10^5 calibration constants defining the alignment system geometry.

For the barrel the oprical system a slightly worse absolute accuracy has been achieved being at the level of 250 μm for Large sectors. For small sectors the alignment is expected to be achieved by using overlapping tracks with large sectors. For this reason a different strategy based on the use of straight tracks for absolute alignment and optical system to follow up movements is chesen for the barrel.

The optical alignment system of the muon spectrometer is an *internal* alignment system, meaning that it provides the positions of muon chambers only with respect to each other, or, equivalently, with respect to an arbitrary coordinate system that is internal to the muon spectrometer. Actually, there are no sensors linking the barrel region to the two end-caps, or the two end-caps to each other, and thus there are three, rather than one, of those arbitrary coordinate systems: one for the barrel and one for each of the two end-caps. This is sufficient as long as the muon spectrometer is used solely for the standalone reconstruction of muon tracks. As soon as tracks are to be extrapolated to other detector components, it becomes necessary to determine the external alignment, i.e. the positions of the three parts of the muon spectrometer with respect to the global ATLAS coordinate system as defined by the inner tracking detectors, and this can only be done with tracks. To a good approximation the external alignment of the end-caps can be obtained from optical surveys of the two outermost wheels of muon chambers while the detector is closed for data-taking; no barrel chambers are visible for a survey at this point, however.

7.1 End-cap alignment

The end-cap muon chambers and their alignment system were installed and commissioned in the ATLAS cavern during the years 2005–2008, and continuous alignment data-taking with the completed system started in summer 2008. The commissioning of the alignment system was a time-consuming and labor-intensive process, and included the positioning of the chambers (with an accuracy of about 5 mm within wheels, and up to 25 mm displacements of entire wheels), clearing obstacles like cables and pipes from optical lines, and repairing or replacing damaged sensors. After commissioning, more than 99% of all relevant alignment sensors were functioning, and only very few failed during the several months of data-taking in 2008. The effect of the missing sensors on the final alignment quality was negligible.

The alignment (i.e. the position coordinates, rotation angles, and deformation parameters of the precision chambers) is reconstructed by a global χ^2 minimization procedure. The total χ^2, as well as the contributions of the individual sensor measurements to χ^2, i.e. the pulls, can be used to estimate the alignment quality from the internal consistency of the fit: if the observed sensor resolutions agree with the assumed ones, one expects approximately $\chi^2/\mathrm{ndf} = 1$ and a pull distribution with zero mean and unit width. Figure 23 shows the observed and expected pull distributions in the end-caps, obtained by assuming design resolutions for all sensor types. In a second step, the assumed sensor resolutions are adjusted until the observed pull distributions, broken down by sensor type, agree with the expected width. This yields the observed sensor resolutions, which are used as input to a Monte-Carlo simulation of the alignment system. The simulation predicts a sagitta accuracy of about 45 μm, and thus, judging by this method, the design performance of 40 μm is nearly reached.

Validating the alignment as reconstructed from the optical sensor measurements requires an external reference. During chamber installation, surveys of the completed end-cap wheels were performed using photogrammetry, and chamber positions from the alignment system agreed with the survey results within 500 μm, the quoted accuracy of the survey. While establishing confidence in the optical system, this type

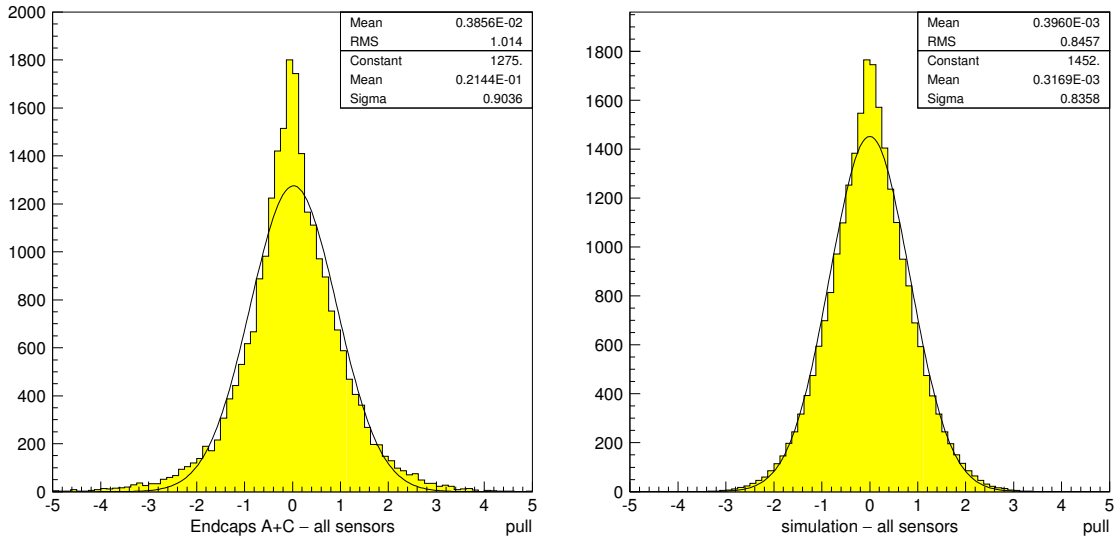

Figure 23: The observed (left, from data) and expected (right, from simulations) pull distributions for the end-caps, assuming design resolutions for all sensor types. Correlations and weakly constrained degrees of freedom cause the expected distribution to have a width below unity. The observed χ^2/ndf is 1.4, the expected one 1.0.

of checks is limited in scope and accuracy, and the full validation of the alignment can only be done with muon tracks. Thus, cosmic muons recorded during magnet-off running of the ATLAS detector were used to cross-check the alignment provided by the optical system. For a perfect alignment, the reconstructed sagitta of straight muon tracks should be zero for each MDT EI-EM-EO measurement tower (when averaged over many towers the mean value can be accidentally compatible with zero despite single towers being significantly misaligned). The observed width of the sagitta distribution is, for cosmic muons, dominated by multiple scattering. A shifted and/or broadened distribution would indicate imperfections of the alignment. We select triplets of segments in the three wheels EI-EM-EO, requiring the three segments to be in the same sector and assigned to the same reconstructed track. Basic segment quality cuts (χ^2/ndf < 10, and at most one expected hit missing per chamber) are applied. The difference in pointing angle between the segments and the track (actually the straight line joining the segments in the two outer wheels, EI and EO) is required to be below $5(50)$ mrad in the precision (second) coordinate, and at least one trigger hit in the phi coordinate has to be associated to the track in order to ensure a good measurement of the second coordinate. About 1700 segment triplets passing all selection cuts are found in the sample consisting of run 91060.

Figure 24 left shows the observed sagitta distributions before and after applying alignment corrections (i.e. the chamber positions, rotations, and deformations as determined by the optical system, as well as a correction for the gravitational sag of the MDT wires) for the two end-caps. Figure 24 right shows the corresponding differences in pointing angle in the precision coordinate between each of the segments and the track (the straight line joining the EI and EO segments). For this plot, the aforementioned cut at 5 mrad was omitted. The improvement in both variables is clearly visible, and the mean value of the corrected sagitta distribution as obtained from the fit of a double-Gaussian function is (-33 ± 42) μm (statistical error only), and thus perfectly compatible with zero within the 45 μm error estimated above from the internal consistency of the alignment fit. The width of the corrected sagitta distribution agrees approximately with expectations for the typical energies of cosmic muons in ATLAS. The width of the corrected angle-difference distribution, on the other hand, is about twice as large as expected: this is mainly a consequence of the additional time jitters on MDT measured drift times described in Section 5

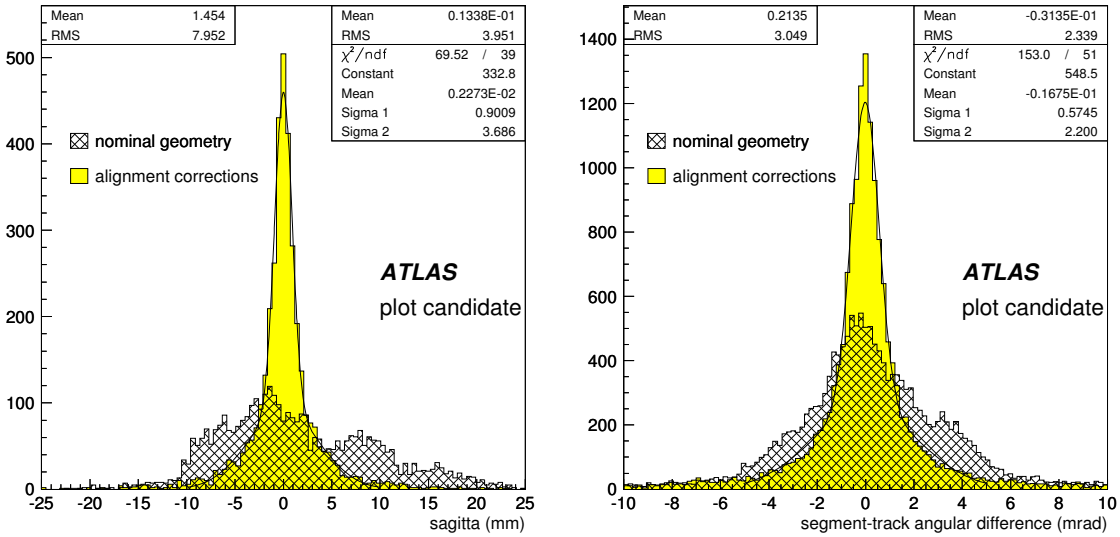

Figure 24: Left: measured sagitta distribution for the two end-caps. The cross-hatched histogram shows the sagitta before alignment corrections, thus reflecting the accuracy of chamber positioning in the ATLAS cavern. The filled histogram shows the sagitta after applying alignment corrections, and the curve is the fit of a double-Gaussian function. Right: measured difference in direction in the precision coordinate between the segments and the track (straight line) which they are associated to. Each segment triplet contributes three entries, and a cut at ± 5 mrad is applied for producing the sagitta plot on the left.

that deteriorates the segment spatial resolution.

Dividing the two end-caps, the mean values of the sagitta distribution are (-30 ± 61) µm on side A and (-37 ± 57) µm on side C. The sign of the sagitta is defined in such a way that most of the conceivable systematic errors and mistakes in the optical alignment reconstruction would cause deviations from zero with the same sign on sides A and C. The analysis is statistics-limited at this point (with a significant fraction of the full 2008 data already included), and breaking it down further to the sector level or even the single-tower (projective chamber-triplet) level (which gives the best sensitivity to the alignment) would require a significant increase in statistics.

We conclude that, with the mentioned caveat concerning the limitations of the analysis, using straight tracks as a cross-check confirms the chamber positions as given by the optical alignment system within the estimated sagitta errors, indicating that the optical system works, and that the design accuracy has nearly been reached in the end-caps. It also shows that the system produces reliable estimates of the uncertainty of the alignment corrections it provides.

7.2 Barrel alignment

7.2.1 Optical Alignment status

Also the Barrel of the MS is equipped with an optical system [15] that was used to provide the 2008 cosmic data reconstruction with alignment corrections.

The installation and commissioning of the barrel optical system has started in 2005 and that followed the installation of the MDT chambers in the pit until 2008. At the time of the recording of the cosmic data described in this note, the barrel optical system was fully installed and 99.7% of the sensors were functioning correctly. Table 7.2.1 summarizes the status of the installed sensors. The complete system is read out continuously, at a rate of one cycle of the 5800 sensors in about 20 minutes. The readout was functioning correctly during the complete period of acquisition of cosmic data.

Type	Total	Working	Broken
Projective	117	117	0
Axial	1036	1031	5
Praxial	2010	2008	2
Reference	256	253	3
CCC	260	260	0
BIR-BIM	32	32	0
Inplane	2110	2101	9
Total	5817	5798	19
%		99.7	0.3

Table 4: Observed status of the barrel optical system, as of 2008-10-19. The sensor categorized as "broken" are those for which no measurement could be recorded.

The alignment reconstruction consists in determining the chambers positions and orientations (referred to as "alignment corrections" in this note) from the optical sensors measurements. This process requires the precise knowledge of the positions of the optical sensors with respect to the sensitive devices of the MDT, i.e. the wires. For that purpose the optical sensors are calibrated, their mechanical extensions measured, and the platforms on which they are attached are glued precisely with respect to the wires. However the early design of the barrel optical system suffers from a few number of errors that eventually dominate the precision of the alignment corrections that can be reconstructed. Furthermore, the only devices giving projective information in the small sectors are the CCC sensors, which are designed for providing the 1 mm accuracy. (The alignment of the small sectors during physics runs is, by design, based on tracks.)

The alignment corrections discussed in this paper cover the 9 upper sectors (01 to 09). The complete period of cosmic data-taking is split in intervals of 6 hours, for which alignment corrections are reconstructed using the optical sensors measurements recorded in that interval. This allows to monitor significant movements of the spectrometer, such as when the magnetic field in the toroids is switched on (average effect of about 500 μm on the sagitta.)

The barrel alignment reconstruction is based on the minimization of a χ^2, whose ingredients are the following, for each optical sensor i:

- the recorded response $\mathbf{r}_i$ of the sensor i,
- a model $\mathbf{m}_i(\mathbf{a})$, which is the prediction of the response of sensor i depending on the alignment corrections $\mathbf{a}$,
- and the error σ_i, which is on the model $\mathbf{m}_i$ estimated uncertainty.

The critical part is the model $\mathbf{m}_i$, as it combines all the knowledge of the precise geometry of the optical sensors (calibrations, platform positions, etc.)

The free parameters in the fit are the alignment corrections $\mathbf{a}$, and in some cases additional parameters used to model the effect of an imprecise sensor platform gluing (e.g. along the MDT tube direction) or a missing sensor calibration. For all these additional parameters, appropriate constraints are included in the fit, that reflects the best knowledge of the above mentioned problems. Overall, 4099 parameters are fitted simultaneously. The fit technique is based on a linear least square, optimized through the use of the sparse matrix library from ROOT [16]. The total reconstruction time for the full barrel is less than 1 minute.

The errors σ_i that are assigned to the various types of sensors are the following:

- Praxial and axial sensors, corrsponding to optical lines conecting MDT chambers on the same Large sector along z-coordinate, are assigned to have a 100 μm precision. This performance is confirmed by precise mechanical measurements of the distance between neighboring chambers.

- The measurements from the reference system are complemented with in-situ distance-meter measurements, leading to a 1 mm precision for the reference system, consistent with the design.

- The projective system, corresponding to optical lines connecting triplet of chambers BI-BM-BO in the same Large sector, is assigned a 200μm precision, consistent with the residuals observed at the end of the fit.

- The CCC sensors, corresponding to optical lines connecting Small sector chambers to the adiacent Large sector ones, are given a resolution of 1 mm. The poor precision of these devices is the main limiting factor for the alignment of the Small sectors.

The praxial and axial sensors suffer from a design problem such that it is quite easy for the operators to mount the sensors with a slight shift (from 100 μm to 1 mm) with respect to the normal position. From praxial residuals, it has been estimated that $\sim 10\%$ of the praxial pairs suffer from this problem. This problem is accounted for by including an additional degree of freedom in the fit modeling the bad mounting, for a selected set of praxial pairs which show large residuals. This additional parameter has a negative impact on the alignment performance. For this reason in the Barrel the planned alignment strategy is slightly different than in the End-cap: dedicated runs without toroidal magnetic field will be used to get an initial alignment of the Barrel muon stations with a precision at the level of 30 μm; then the optical alignment system will be used to follow up station movements due toe the switching on of the toroidal field and temperature effects, the so called *relative mode* already tested in the MS system test-beam performed at CERN in 2002–2003 [4, 5]. After the minimization, the value of χ^2/ndf is 1.9, which shows that the sensors errors are overall slightly underestimated.

7.2.2 Expected Performance of optical alignment in the Barrel

Similrly to what is done in the End-cap an approximate estimate of the performance of the alignment system may be inferred from the χ^2, using the following formula, where θ_i are the fitted parameters and V is the global error matrix over all the fitted parameters (of size 4099×4099):

$$(V^{-1})_{ij} = \frac{1}{2}\frac{\partial^2\chi^2}{\partial\theta_i\partial\theta_j}\Big|_{\hat{\theta}}. \tag{2}$$

The performance of the alignment system in terms of sagitta may be estimated by generating lines interpreted as tracks, originating from the interaction point and traversing three layers of chambers. The sagitta of these pseudo-tracks is a function of some of the alignment corrections, and thus the formula of error propagation may be used to infer the contribution from the alignment to the error on the sagitta of these pseudo-tracks. This technique relies on the fact that the errors of the optical sensors should be correctly estimated, and thus that the χ^2 is correctly normalized. As this is not the case ($\chi^2/ndf = 1.9$), we should trust the results only as a rough estimation of the performance of the optical alignment.

The result is shown in Fig. 25: the Small sectors have a significantly worse alignment than the Large sectors, as expected from the system design (due to the expected performance of the CCC sensors).

Conservatively, we conclude that the performance in terms of sagitta precision of the optical system is ~ 200 μm for the Large sectors, and ~ 1 mm for the Small sectors.

7.2.3 Straight track alignment

In order to bring the performance of the Barrel alignment system to the design one and to validate the optical alignment corrections in relative mode, straight muon tracks with the toroid magnet switched off will be used. The straight tracks will be used to determine in absolute mode the *initial* spectrometer geometry. Once this geometry is determined the optical alignment system can trace all chamber displacements in a relative mode.

To align the Barrel part of the muon spectrometer with straight tracks an alignment algorithm has been developed [13]. The alignment procedure is based upon the *Linear Least Squares Fits with a Large Number of Parameters* (MILLEPEDE) method [14]. This method uses both alignment and track parameters inside a global fit. As a result all correlations between alignment and track parameters are taken into account and the alignment algorithm becomes unbiased.

The performance of the straight track alignment algorithm has been tested with both Monte Carlo and cosmic muons collected during the ATLAS commissioning runs. The simulation based studies have shown that 10^5 muon tracks with a momentum of at least 20 GeV crossing the detector interaction point are enough to align the Large and Small Barrel sectors with a precision of teh order of 30 μm. Small sectors require five times more tracks than large sectors, due to the presence of the toroid magnet coils, which causes a higher amount of multiple scattering.

Using straight cosmic muon tracks recorded during the commissioning run 91060, a track based set of alignment constants has been produced. A total of ten million events have been used corresponding to about 300 thousand cosmic muon tracks per each barrel sector. The statistical uncertainty on the sagitta using the track based alignment procedure was estimated to be 30 μm for Large sectors.

Cosmic run 91060 data have been processed with the muon reconstruction software twice: (1) using optical alignment and (2) using track-based corrections. Both geometries have then been tested by checking track sagitta of projective cosmic muons crossing all three layers of chambers (Inner, Middle and Outer). Only tracks passing close to the ATLAS interaction point in the precision plane have been chosen. Then the hits on the inner and outer chambers have been used in order to fit a straight line, while the residuals of the hits from the middle chambers are plotted on a histogram. In a good approximation the mean value of the hit residuals of the Middle MDT station corresponds to the track sagitta. In case

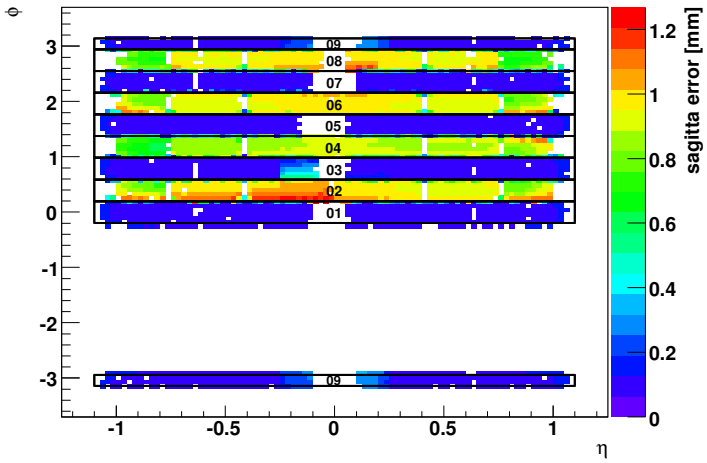

Figure 25: Estimated contribution to the error on the sagitta, coming from the alignment. As expalined in the text this is a rough estimate. as expected from teh systm design the Small sectors are aligned with a significantly worse precision than the Large sectors.

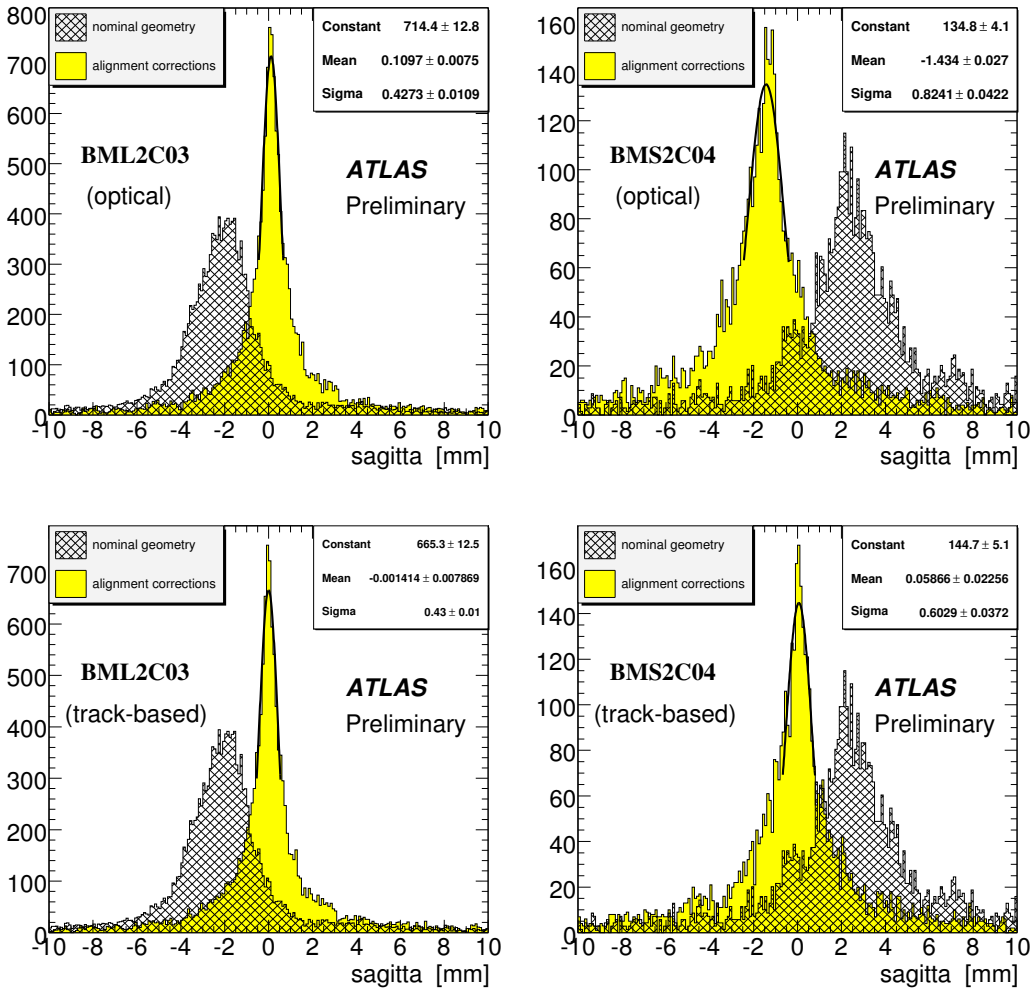

Figure 26: Cosmic track sagitta in the large BML2C03 and small BMS2C04 middle chambers. Top plots have been produced using alignment corrections the optical system only. Bottom plots have been produced with using track-based alignment corrections.

of perfect alignment the mean value of the sagitta is ecpected to be zero for straight tracks.

The results of this cross-check for two geometries are shown in Figure 26 for specific Barrel stations: BML2C03 (Large sector) and BMS2C04 (Small sector). Two upper plots show the performance of the optical alignment corrections, while the lower plots show the same results for track-based alignment corrections. For comparison in all four plots the sagitta distributions given using the nominal geometry (geometry derived from the ATLAS layout) only is also shown. The tails of sagitta distributions are due to the multiple scattering of muons. In Large sector (here BML2C03), the shape of the optical sagitta distributions and the track-based one are almost identical, except that the optical sagitta distributions is centered at about 100 μm. For BMS2C04 (Small sector) the sagitta distribution provided by the optical alignment system is centered at the level of 1 mm as expected.

On the Figure 27 mean values of track sagitta distributions for the muon chambers of Large of the upper sectors 3, 5, and 7 are combined together. Small sectors are presented by sector C04 which was the only small top sector with large statistics that had no problems with the second coordinate

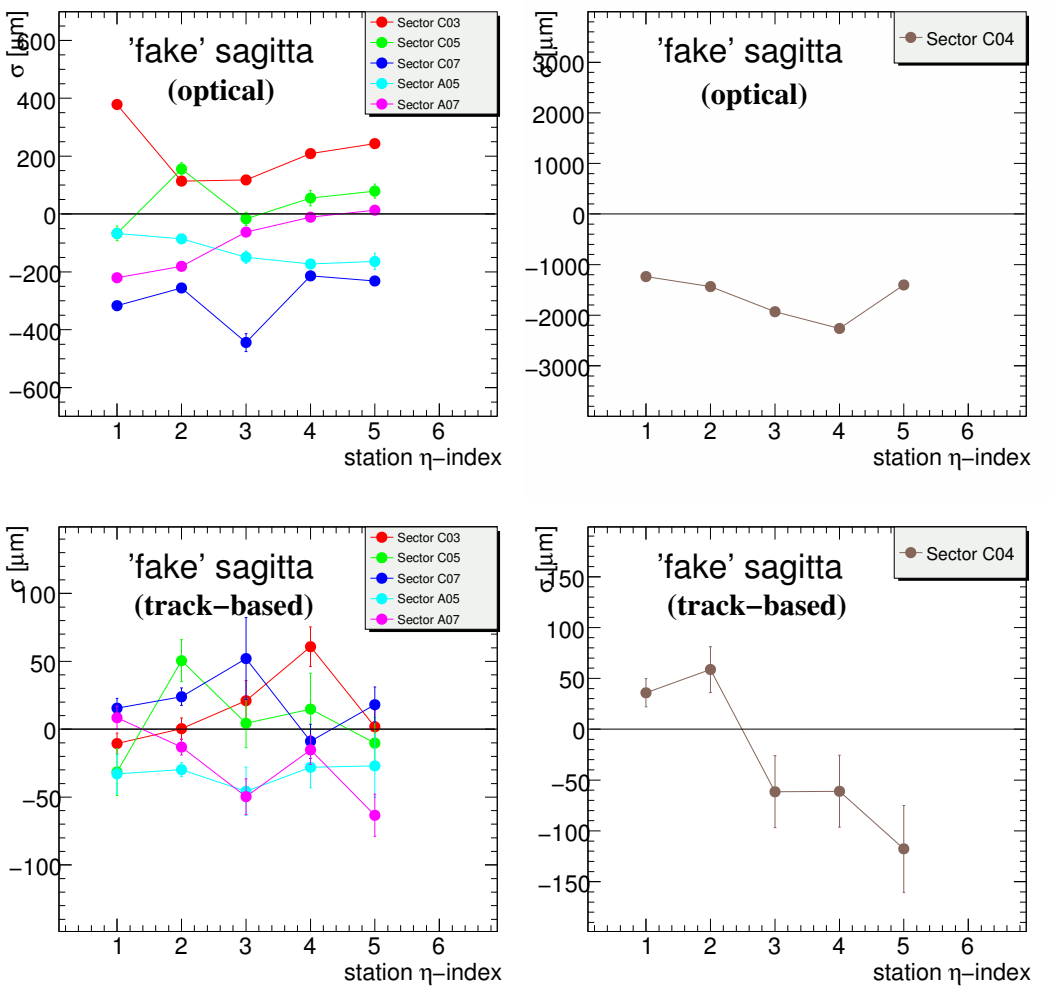

Figure 27: Mean values of cosmic track sagitta distributions provided by optical alignment system alone and provided by track-based alignment. Plots on the left side show the Large top barrel sectors. Plots on the right side are produced for the Small barrel sector C04 (side C, phi angle between 78.75 and 56.25).

measurement during run 91060. For the presented large sectors the optical alignment system alone provides performance at the level of 200 μm. Calibrated with straight muon tracks the optical system will be able to provide alignment close to the required level of 30 μm.

8 Pattern Recognition and Segment Reconstruction Performance

The MS hits are first associated into local segments before a full track fit is performed. In the Moore algorithm segments are reconstructed using patterns as a seed. Patterns are collection of hits selected by applying a straight line Hough transform to the MDT, CSC, RPC and TGC position measurements. Each pattern is characterized by a position and direction and contains all the associated hits. Starting for the patterns the segments are reconstructed with a straight line fit. The t_0 refit as described in Sections 2 and 5 is applied at this stage. To achieve a high segment finding efficiency in cosmic ray events, the MDT single-hit errors has been enlarged to a value of 1 mm, cuts on matching angles were opened and

hit dropping criteria were relaxed. The minimum number of hits per segment was set to 3 and no cuts were applied on the number of missed hits.

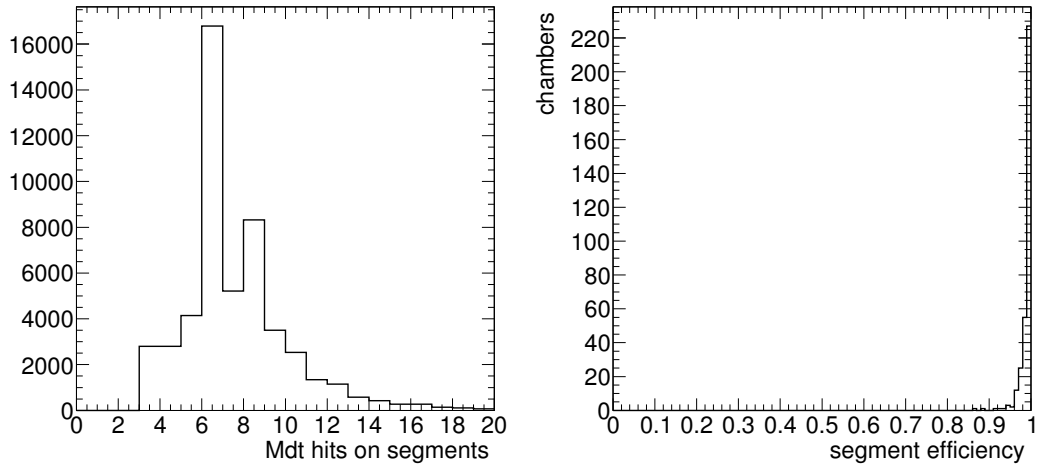

Figure 28: Left: Number of MDT hits per segments for segments associated to tracks. Right: Segment reconstruction efficiency.

In Figure 28 left the number of MDT hits for segments on tracks is shown. In the distribution clear peaks can be observed at 6 and 8 hits corresponding to the 6 (Middle and Outer) and 8 layer (Inner) chambers.

The efficiency of the segment reconstruction is determined in the following way. Firstly, cosmic shower events are suppressed by requiring less than 20 segments in the event. Secondly, reconstructed muon tracks that are expected to cross at least three muon stations layers is required. Muon tracks are reconstructed requring hits in at least two out of the three muon spectrometer layers (ss explained in Section 1 the detector is divided into Inner, Middle and Outer station layers). The track is then extrapolated to each of these layers. Quality cuts are applied on the tracks to ensure that the extrapolation is sufficiently accurate. For each station crossed by the selected track, the presence of a reconstructed segment is checked. It is not required that the hits of this segment are associated to the muon track. The segment efficiency is then obtained for each MDT crossed chamber by the fraction of times a segment is found. In orger to reduce the effect of unistrumented regions of the MS fiducial cut in eta has been applied for both barrel and end-cap. One chamber that was not operational in the analysed run has been removed from the sample. In addition it was not possible to determine the efficiency for all chambers due to limited coverage of the trigger of to the cosmic ray flux.

The distribution of the segment efficiency is shown in Figure 28 right. The results shown here are based upon 322 Barrel and 339 Endcap chambers. The average efficiency is 99.5 %. The average efficiency for the Barrel Inner Chambers is 98.7 %, the Barrel Middle 99.2 %, the Barrel Outer 99.6 %, the Endcap Inner 99.2 %, the Encap Middle 99.8 % and the Endcap Outer 99.9 %. In the efficiency there is a small contribution from geometrical losses in the Barrel feet region and the in magnet support structure of about 0.5%. The Inner Chambers have a slightly lower segment efficiency due to remaining uncertainties in the track extrapolation. The systematic uncertainty on the average efficiency of 99.5 % is estimated to be 0.5%.

In Figure 29 the number of reconstructed segments per event is shown. Only events with at least one segment in the Inner, Middle and Outer station layers are selected in this plot after rejecting cosmic shower events as described above. In order to understand this distribution one has to distinguish several

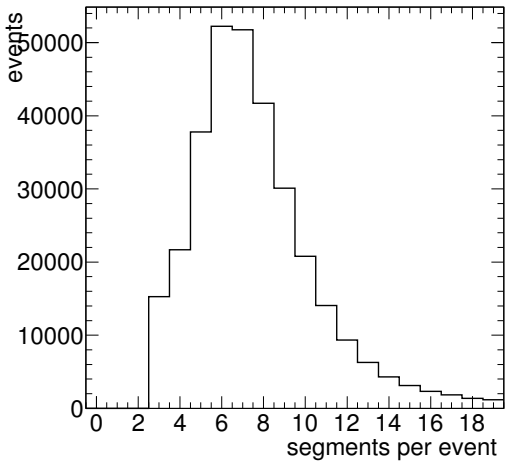

Figure 29: Number of reconstructed segments per event.

contributions:
Segments associated to tracks give an avarage of 5.1 segments per event.
For segments not associated to a track but within a distance of 1 meter two contributions are identified: combinatorics in same chamber (i.e. extra segments made by the pattern recognition) account for 1.0 segments per event. Segments not associated to a track built on a different chamber with respect to the one expected to be cressed by the track amuont to about 1.o segment per event and they are mainly to good segments not associated to a track due to low momentum muons that have a large extrapolation error. Another category are the segments with a distange larger than 1 meter with respect to the coler track. Some of this segments corresponds to real cosmic showers where the additional muon do not cross enough stations to for a full track: these segments have typically 6 or more MDT hits and they give about 0.1 segment per event. The remaining segments with less than 6 MDT hits and more than 1 meter distance from a track include also cosmic showers and segments built with accidantal noise . They account for 0.2 segments per events. This category and the the category of combinatoric are expected to be strongly reduced in real collision when the resolution used to associate hits to segments will be much smaller.

9 Track Reconstruction Studies

The MOORE and Muonboy muon reconstruction programs have been developed and optimized to recinstruct muons originating from the Atlas interaction point in collision events. In order to cope with the different topology of cosmic ray muons they have been slightly modified as explained in Section 2. In this Section some basic performance of the two reconstruction algorithms on cosmic muons are reported.

In order to select an unbiased cosmic ray sample that emulate as much as possible the *collision* muons only events with tracks reconstructed in the ATLAS Inner Detector (ID) have been considered. Events with an ID track that satisfy the following criteria have been selected: at least 20 hits in the TRT detector, twice the nuber of SCT hits plus pixel hits greater or equal to 8, distance of closest approach in the transverse plane (—d0—) and on the z axis (—z0—) smaller that 1m, absolute value of the reconstructed pseudo-rapidity smaller than 1, normalized $\chi^2/ndf < 3$. All the results showed in the following refers to cosmic-ray events that pass this selection.

In order to mimic muons from collision, the tracks reconstructed in the spectrometer are splitted at

their perigee (point of closest approach to the beam axis), giving usually two reconstructed tracks, one in the upper part of the spectrometer and one in the lower part. An important quantity related to the

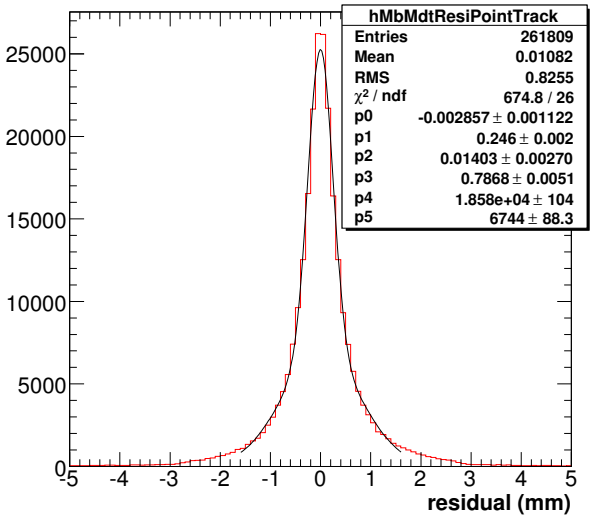

Figure 30: Residual of MDT hits. The fit superposed is a sum of two Gaussian, which about the same normalization. The narrow one has a width of 250 microns, while the wider one has about 800 microns.

quality of the reconstruction are the residuals of the MDT hits, defined as the difference between the measured radius and the minimum distance of the track to the wire. As the MDT hit was itself used for the track fit, the study is restricted to tracks crossing at least three stations in order to better constrain the track and to keep small the weight of any hit in the track prediction. The residuals of MDT hits on tracks reconstructed with one of the two algorithm are shown in Figure 30. The residuals have been fitted with a double-Guassian function and a narrow standarddeviation of about 250 μm and a wide one of about 800 μm are found. Compared to the segment residuals shown in Section 6.1 two additional effects contribute to the degradation of the standard deviation: the misalignment between stations and multiple scattering in the MS material.

The reconstruction efficiency has been computed as the fraction of events where a muon tracks is reconstructed in the MS Top or Bottom hemisphere once an Inner Detector track has been found with the selection criteria described above. In addition a momentum cut of 5 GeV (9 GeV) on the Inner Detector track is applied to compute the Top (Bottom) hemisphere efficiency. The results obtained are shown in Figure 31 as a function of the pseudo-rapidity η reconstructed by the Inned Detector for top and bottom sector tracks separately. As expected most of the inefficiencies are concentrated at regions of eta close to zero that corresponds to the unistrumented region of teh MS due to the presence of the gap for the services of the detector. The integrated values for the efficiency are of 95.2% for teh Top and 94.5% for the Bottom hemisphere respectively. If the four central bins in eta are removed from the efficiency computations these values increases to 98% and 96% respectively. The lower value for the Bottom part is explained by the presence of unistrumented regions corresponding to tha ATLAS feet.

In runs with the toroid magnets switched on, like in run 91060, the cosmic ray muon momentum spectrum has been measured by the MS and it is shown in Figure 32 left. The difference between positive and negative muons spectra is due to the different incoming fluxes.

For events where the both branches (Top and Bottom hemispheres) of the track are reconstructed, the two values of the momentum measured in the MS can be compared. This is shown in Figure 32 right

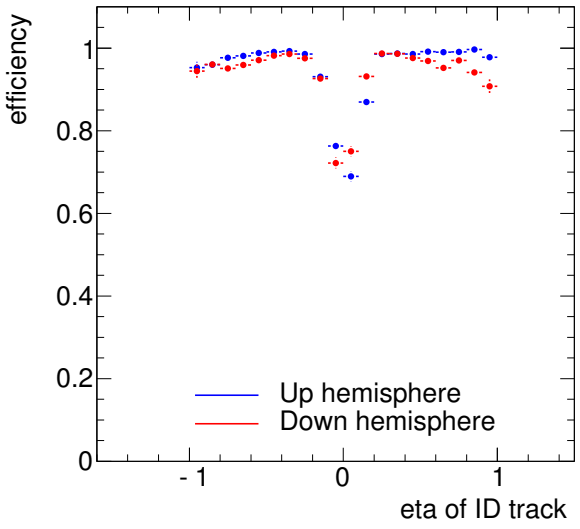

Figure 31: Muon Spectrometer track reconstruction efficiency as a function of the pseudo-rapidity. The Inner Detector track are used as *tag* muons as explained in the text.

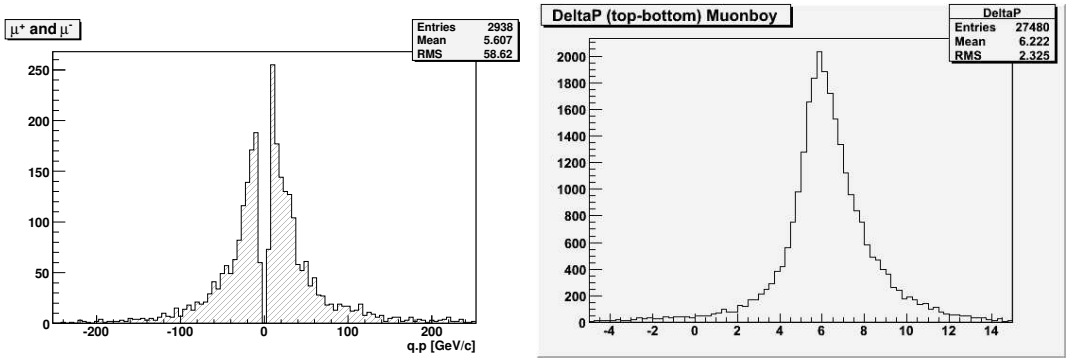

Figure 32: Left: Cosmic ray muon momentum spectrum as measured by the spectrometer, with a cut at 5 GeV. Right: Difference between the momentum measured in the upper hemisphere and the one measured in the lower hemisphere. Only tracks with momenta bigger than 15 GeV are shown.

where the measured momentum, extrapolated to the external surface of the calorimeter, Top–Bottom difference is shown. As the muon crosses twice the calorimeter thickness between these two points, we expect an energy loss of about 6 GeV in agreement with the measured value.

10 Conclusions

The cosmic data collected in the 2008-2009 ATLAS cosmic runs have analyzed to asses the Muon Spectrometer performance after installation in the ATLAS experiment. Results on several important aspects of the Muon Spectrometer performance have been presented including detector coverage, data quality, precision and trigger chamber performance, calibration, alignment and track reconstruction. The detector coverage durig these runs has been higher than 99% with the exeption of the RPC detector being still under commisisoning. For this detector the detector the coverage has steadily improved in the 2008–2009 period reaching in spring 2009 the 97% level. The basic detector performance in terms of hit efficiency and resolution for MDT, RPC and TGC chambers have been measured and found in agreement with results obtained from past test-beam measurements. A slight deterioration of MDT spatial resolution due to additional time jitters present in cosmics, partially recovered with dedicated algorithms, has been observed in agreement with expectations. The alignment performance of the End-cap and Barrel optical system have been measured using cosmic tracks without toroidal field. From the results it can be cloncluded that while for the End-cap the optical system alone is able to provide the required precision on alignment corrections for the Barrel the additional constraints from staright tracks runs will be needed. The reconstruction software has been modified to cope with cosmic rays. With these changes the segment and track reconstruction efficiency have been found to be very close to he value expected from the geometrical acceptance of the Muon Spectrometer.

Acknowledgments

References

[1] *The ATLAS Muon Spectrometer Technical Design Report*, The ATLAS Muon Collaboration, CERN/LHCC/97-22, 31 May 1997.

[2] *The ATLAS Experiment at the CERN Large Hadron Collider*, The ATLAS Collaboration, G Aad et al 2008 JINST 3 S08003.

[3] *Expected Performance of the ATLAS Experiment : Detector, Trigger and Physics* The ATLAS Collaboration, G Aad et al., CERN-OPEN 2008-020

[4] *System Test of the ATLAS Muon Spectrometer in the H8 Beam at the CERN SPS*, C. Adorisio et al., Nucl. Instrum. Meth. A 593 (232-254), 2008

[5] *Study of the ATLAS MDT spectrometer using high energy CERN combined test beam data*, C. Adorisio et al., Nucl. Instrum. Meth. A598 (400-415), 2009

[6] The ATLAS collaboration, *ATLAS Computing Techincal Design Report, ATLAS TDR-017, CERN-LHCC-2005-022.*

[7] S. Hassani et al., *A Muon identification and combined reconstruction procedure for the ATLAS detector at the LHC using (Muonboy, STACO, MuTag) reconstruction packages",NIM A572, 2007, pages 77-79.*

[8] P.Branchini, F.Ceradini, S. Di Luise, M.Iodice, F.Petrucci, IEEE Transaction on Nuclear Science 55 (2008) 620-627

[9] Drift Time Spectrum and Gas Monitoring in the ATLAS Muon Spectrometer Precision Chambers, Nucl. Instr. and Meth. A588, 347-358 (2008)

[10] GARFIELD - Simulation of gaseous detectors, Rob Veenhof, CERN Program Library W5050.

[11] C. Guyot et al., The Alignment System of the Barrel Part of the ATLAS Muon Spectrometer, ATLAS Note ATL-MUON-PUB-2008-007 (2008).

[12] S. Aefsky et al., The Optical Alignment System of the ATLAS Muon Spectrometer Endcaps, JINST 3 P11005 (2008).

[13] Igor Potrap, Oliver Kortner, Sergey Kotov, Hubert Kroha. *Alignment of the ATLAS muon spectrometer with straight tracks using MILLEPEDE method*, COM-MUON-2007-017

[14] V.Blobel, *Millepede: Linear Least Squares Fits with a Large Number of Parameters.* Available at: http://www.desy.de/˜blobel/mptalks.html

[15] J.-C. Barrire et al, *The alignment system of the barrel part of the ATLAS muon spectrometer*. ATL-MUON-PUB-2008-007, ATL-COM-MUON-2008-002, Jan 2008.

[16] Rene Brun and Fons Rademakers, *ROOT - An Object Oriented Data Analysis Framework*, Proceedings AIHENP'96 Workshop, Lausanne, Sep. 1996, Nucl. Inst. & Meth. in Phys. Res. A 389 (1997) 81-86. See also http://root.cern.ch/.